Enantiodivergent Biosynthesis of β-Hydroxy esters by Self-Sufficient Heterogeneous Biocatalysts in Continuous Flow.

Daniel Andrés-Sanz [a], Ainhoa Maiz-Iginitz, [a,b] Juan M. Bolivar, [c] Alejandro H. Orrego,[a] Haritz Sardon,[b] and Fernando López-Gallego*[a,d]

a. *Heterogeneous Biocatalysis Laboratory, Center for Cooperative Research in Biomaterials (CIC biomaGUNE), Basque Research and Technology Alliance (BRTA), Paseo de Miramón 182, Donostia San Sebastián, Spain*

b. *POLYMAT and Department of Polymers and Advanced Materials: Physics, Chemistry and Technology, Faculty of Chemistry, University of the Basque Country UPV/EHU, Paseo Manuel de Lardizábal, 3, 20018 Donostia-San Sebastián, Spain*

c. *FQPIMA Group Department of Chemical Engineering, Complutense University of Madrid, Madrid, Spain*

d. *IKERBASQUE, Basque Foundation for Science, María Díaz de Haro 3, 48013 Bilbao, Spain*

*Corresponding author
Fernando López-Gallego: flopez@cicbiomagune.es

Abstract

β-Hydroxy esters are essential building blocks utilised by the pharmaceutical and food industries in the synthesis of functional products. The asymmetric reduction of β-keto esters using cell-free enzymes presents a viable approach to manufacture enantiomerically pure β-hydroxy esters. However, the unbearable economic costs underlying enzymes and cofactors call for innovative approaches to maximize their reusability. Herein, we develop two self-sufficient Heterogeneous Biocatalysts (ssHBs) for the enantiodivergent reduction of β-keto esters to yield enantiomerically pure β-hydroxy esters. A thermophilic (*S*)-3-hydroxybutyryl-CoA dehydrogenase from *Thermus thermophilus* HB27 (TtHBDH) and an (*R*)-specific ketoreductase from *Lactobacillus kefir* (LkKRED) are selected, kinetically characterised, and immobilised onto macroporous agarose beads. Finally, the immobilised enzymes are coated with cationic polymers to co-immobilise the required redox cofactors. The resulting ssHBs catalyse the asymmetric reduction of β-keto esters without the exogenous supply of NAD(P)H and using 2-propanol as an ancillary electron donor. Then, we construct two enantiodivergent packed bed reactors (PBRs) integrating these two ssHBs and determine their optimal operational parameters through condition screening and kinetic simulations. The ssHBs in continuous flow operation exhibit good operational stability, illustrated by a maximum Space-Time Yield (STY) of 49.5 g L^{-1} h^{-1} for the continuous production of enantiopure ethyl 3-(*R*)-hydroxybutyrate over 21 days. Under these conditions, LkKRED and NADPH achieve total turnover numbers of 9.3 x 10^5 and 2.7 x10^4, respectively. Upon mass metric analysis, we conclude that these ssHBs meet the efficiency and sustainability standards to be implemented in some industrial processes, advancing the concept of self-sufficient biocatalysis for process intensification.

Keywords: Flow biocatalysis, enzyme immobilisation, NAD(P)H recycling, dehydrogenases, asymmetric reduction.

2

INTRODUCTION

β-hydroxy esters represent a family of high-value building blocks for the chemical industry. The chirality of their hydroxyl group plays a pivotal role in their functional properties and applications. For example, ethyl (*S*)-4-chloro-3-hydroxybutyrate is a chlorinated ester present as an intermediate in the synthesis of statins,[1] but also methyl 3-hydroxybutyrate is a promising active pharmaceutical ingredient to treat Alzheimer's disease[2] and memory loss prevention.[3] Moreover, β-hydroxy esters find use in the synthesis of insect pheromones[4] and other bioactive compounds.[5-7] Finally, β-hydroxy (thio)esters and their corresponding acids are key intermediates in the biosynthesis of polyhydroxyalkanotes (PHAs) of different nature.[8, 9]

Multiple chemical routes are available for the synthesis of β-hydroxy ester or acids,[10] where aldol condensations,[11-13] Reformatsky reactions,[14-16] and epoxide opening reactions dominate among others. However, the enantioselectivity of these methods is limited. Alternatively, Noyori asymmetric hydrogenation of ketones[17, 18] yields excellent enantiomeric excesses using metal catalysts under harsh conditions yet limits the process sustainability. To overcome some of the issues underlying the current chemical process, biocatalytic asymmetric reduction of prochiral ketones emerges as a sustainable and often more efficient alternative to conventional chemical methods. The use of biodegradable biocatalysts can lead to efficient processes with high regio and enantioselectivity under mild reaction conditions.

Bio-based production of β-hydroxy esters is mainly based on fermentations using different microorganisms harbouring native or expressing heterologous alcohol dehydrogenases.[19-21]. In particular, the asymmetric reduction of **1a** into (*S*)-ethyl 3-hydroxybutyrate catalysed by Baker´s yeast whole-cells achieves a conversion exceeding 90% and enantiomeric excess of 95%[22]. Enzyme mining and engineering has given rise

to a myriad of enzyme variants with exquisite enantioselectivity and high activity for the synthesis of chiral β-hydroxy ester or acids.[23-25] Another classic route for the synthesis of 3-(R)-hydroxybutyric acid[26] or their corresponding ester derivatives is the enzymatic hydrolysis of PHBs produced by microbes. Despite the high potential of whole-cell biocatalysts in multi-step reactions and particularly for the biosynthesis of β-hydroxy esters, the metabolic background of engineered microbes leads to low-purity products, and cell adaptation to the new environment burdens the process reproducibility.

The use of cell-free biocatalytic systems overcomes these major disadvantages of whole-cell biotransformations, increasing the purity of products yet the price of enzymes and cofactors, their low operational stability and their difficulty to be reused hurdle to embrace these processes under industrial environments.[27-29] Cost optimization inbiochemical processes is based on the efficient reuse of enzymes and cofactors. This is achieved by enzyme immobilization, as well as by managing cofactors through various recycling methods, such as retention using membrane reactors or Pickering emulsions or recovery and re-use by implementing extraction processes.[30-34] As a solution to increase the robustness of cell-free biocatalytic systems, enzyme and cofactor immobilisation on solid supports enables their reutilisation in different reactor configurations (flow and batch) and typically enhances their storage stability and their operational lifespan.[30, 35] However, finding the suitable immobilisation protocol to co-immobilise enzyme and cofactors recovering high activity and stability is not trivial, so a variety of immobilisation chemistries and conditions must be screened to maximise the overall performance of the resulting heterogeneous biocatalysts. When both enzymes and cofactors are co-immobilised, these heterogeneous biocatalysts become self-sufficient as no cofactor must be exogenously added during the process.

4

In this approach, carrier surfaces undergo functionalization with positively charged amine groups capable of electrostatically binding phosphorylated cofactors. Enzymes become irreversibly attached to the carrier surface, while cofactors are reversibly adsorbed, establishing an association-dissociation equilibrium primarily driven by electrostatic interactions with the polymeric matrix. This equilibrium facilitates the continuous movement of cofactors between the active centres of enzymes without being lixiviated from the carrier particles.

Having methodologies to prepare these self-sufficient biocatalysts (ssHB) is highly relevant to enable the use of costly cofactor that otherwise restricts the industrial implementation of cofactor-dependent enzymes. Our group has successfully developed a technology for co-immobilizing phosphorylated cofactors with their respective enzyme partners through reversible ionic interactions that enable the access of the co-immobilised cofactors to the active sites of the immobilised enzymes.[36] Through this strategy, we implemented a diversity of NAD(P)H-dependent oxidoreductases[37] and PLP-dependent transaminases[38] into ssHBs that drive chemical processes where the co-immobilised enzymes and cofactors can be simultaneously reused.[39] In this context, the application of ssHBs in flow through their integration into packed bead reactors offers some advantages compared to discontinuous batch reactors like paralleling or telescoping reactors for multi-step reactions, reduction of enzyme inactivation due to attrition caused by stirring conditions and easy reactor parametrisation and monitorisation. [40]

In this work we report the kinetic parameters of a thermophilic (*S*)-selective 3-hydroxybutyryl-CoA dehydrogenase from *Thermus thermophilus* HB27 (TtHBDH)[41] and an (*R*)-selective ketoreductase from *Lactobacillus kefi*r (LkKRED)[42] for the asymmetric reduction of nine β-keto esters (Scheme 1, **1a-i**) into their corresponding β-hydroxy esters (**2a-i**). Our experience to co-immobilise TtHBDH with NADH that affords a *S*-selective

ssHB[41] aided us to co-immobilise LkKRED with NADPH and fabricate an enantiocomplementary *R*-selective ssHB. Then, we packed these two ssHBs into plug-flow columns to set two enantiodivergent packed bed reactors (PBR) for the continuous biosynthesis of enantiopure **2a** as model product, for which different flow rates and substrate concentrations were evaluated to find the optimal operation conditions. Supported by kinetic simulations, we shined light on the behaviour of these ssHBs under continuous operation. Finally, we found out that the operational stability of the ssHB depends on the operation temperature which dramatically affects the chemical stability of the immobilised cofactor. To conclude, we compared the flow performance of these two ssHBs with other ssHBs reported in the literature and determined their mass and sustainability metrics as industrial biocatalysts.
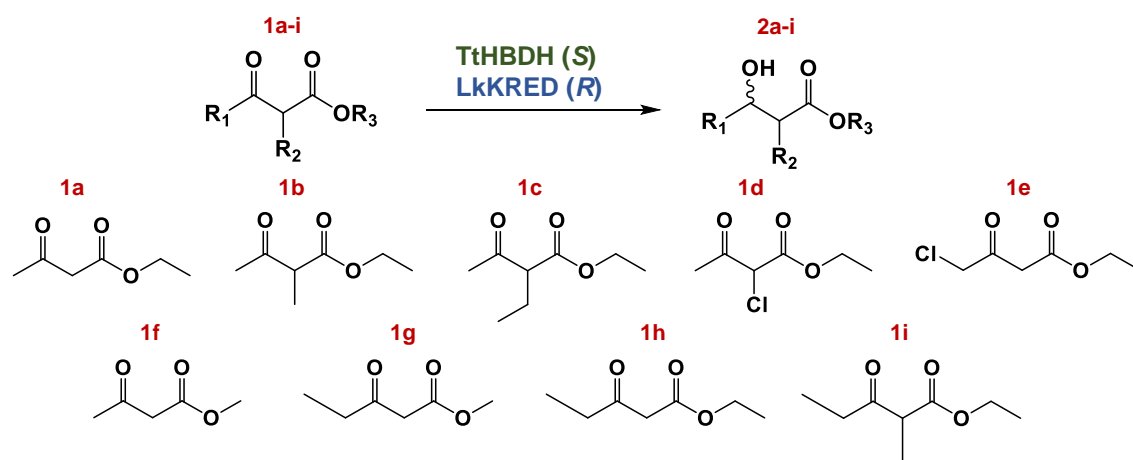
Figure 1. Scheme of the asymmetric reduction of different alkyl (R3) β-keto esters substituted at C2 (R2) and C4 (R1) with diverse groups. The reaction is catalysed by two enantiodivergent enzymes; (*S*)-selective 3-hydroxybutyryl-CoA dehydrogenase from *Thermus thermophilus* HB27 (TtHBDH)[41] and an (*R*)-selective ketoreductase from *Lactobacillus kefi*r (LkKRED).[42]

RESULTS AND DISCUSSION

Substrate scope and kinetic characterisation of dehydrogenases for the asymmetric reduction of β-keto esters.

Our goal was to efficiently synthesize both enantiomers of various β-hydroxy esters using continuous flow processes. To accomplish this, we sought out highly enantioselective enzymes that complement each other for the asymmetric reduction of β-keto esters. For the *S*-selective pathway, we opted for 3-hydroxybutyryl-CoA dehydrogenase (TtHBDH) from *Thermus thermophilus* HB27,[41] which exhibited outstanding enantioselectivity for ethyl 3-ketobutyrate. As the *R*-selective enzyme, we selected ketoreductase from *Lactobacillus kefir* (LkKRED), [42] known for its high *R*-enantioselectivity across a range of substituted ketones (**Table S1**).

With these enzymes in hand, we initially determined the Michaelis-Menten parameters for free enzymes using nine chemically diverse β-keto esters (**Figure 1**). Spectrophotometric assays were conducted to measure the reductive activity of both TtHBDH and LkKRED at different substrate concentrations (**Figure S1-S2**). From Michaelis-Menten plots, we determined all kinetic parameters for both free enzymes (**Table 1**). TtHBDH exhibited a wide range of k_{cat} values (0-26 s^{-1}) for different β-keto esters, with the best substrate being **1d** and the worst being **1i**, under pH 7 and 30º C conditions. Notably, TtHBDH displayed high k_{cat} values for alpha-branched β-keto esters with small substituents (**1b**). Furthermore, this thermophilic enzyme presented the highest catalytic efficiency values towards chlorinated esters due to the lower K_M values, in line with previous observations. [41] For bulkier group-substituted β-keto esters (**1c**, **1h**, and **1i**), either the catalytic efficiency was low, or the substrate saturation point was not reached (**Figure S1**), indicating a potential space limitation at the active center. In general, TtHBDH exhibited high K_M values for the reduction of β-keto esters, ranging from 20 to

7

734 mM, possibly due to its natural preference for CoA thioesters as substrates. Notably, negligible substrate inhibition was observed (**Figure S1**), allowing for flexibility in working with high substrate concentrations to achieve efficient enzymatic activity.

Under the same conditions (pH 7 and 30 ºC), LkKRED displayed significantly lower K_M values for all β-keto esters than TtHBDH, resulting in superior catalytic efficiency for most substrates. However, some substrates with low K_M values (**1a**, **1d**, **1g**) also exhibited enzyme inhibition (**Figure S2**), except for **1e**, where inhibition was not detected. Under enzyme saturation conditions, LkKRED generally showed lower k_{cat} values for all substrates compared to TtHBDH, except for **1h** and **1i**. Notably, LkKRED was more catalytically effective than TtHBDH for bulkier β-keto esters **1c**, **1h**, and **1i**, while methyl esters (**1f**) were less favourable substrates for LkKRED compared to TtHBDH.

Table 1 Michaelis–Menten steady-state parameters of TtHBDH and LkKRED on different β-keto esters

	V_{max} (µmol min^{-1} mg^{-1})		K_M (mM)		k_{cat} (s^{-1})		K_i (mM)		k_{cat}/K_M (mM^{-1} s^{-1})	
	TtHBDH	*LkKRED*	*TtHBDH*	*LkKRED*	*TtHBDH*	*LkKRED*	*TtHBDH*	*LkKRED*	*TtHBDH*	*LkKRED*
1a	6 ± 1	1.22 ± 0.03	734 ± 117	0.19 ± 0.03	20 ± 3	4.8 ± 0.1	nd	154 ± 27	0.03	24.4
1b	3 ± 1	1.08 ± 0.03	223 ± 72	8.0 ± 0.6	10 ± 3	4.2 ± 0.1	1687	nc	0.05	0.53
1c	nc	1.5 ± 0.4	nc	26 ± 16	nc	5.8 ± 1.7	nc	nc	nc	0.22
1d	8 ± 3	2.5 ± 0.3	21 ± 8	0.49 ± 0.15	26 ± 9	9 ± 1	nc	30 ± 12	1.22	20.2
1e	3.1 ± 0.5	0.77 ± 0.02	55 ± 11	0.79 ± 0.11	9.7 ± 1.6	3.1 ± 0.1	nc	nc	0.18	3.84
1f	1.2± 0.0	nd	156 ± 15	nd	4 ± 0	nd	nc	nd	0.025	nd
1g	0.44± 0.07	1.06 ± 0.06	726 ± 158	1.0 ± 0.1	3.9 ± 0.6	4.2 ± 0.2	nc	33 ± 7	0.002	4.31
1h	nc	0.98 ± 0.25	nc	1.3 ± 0.5	nc	4 ± 1	nc	nc	nc	2.98
1i	nc	0.85 ± 0.04	nc	35 ± 3	nc	3.4 ± 0.2	nc	nc	nc	0.094

Table 1. nc= parameters could not be calculated because either an activity plateau was never reached, or substrate inhibition was not detected. nd = Activity non detected. The kinetic parameters were determined by spectrophotometric enzymatic assay at pH 7 and 30 °C. The general enzymatic assay involved the reduction of a solution containing different substrate concentrations (0.1-500 mM) in the presence of 0.2 mM of NADH or NADPH in 25 mM sodium phosphate buffer at pH 7. Further information in materials and methods.

In summary, these enzymes are complementary in their enantiopreference but also in their substrate scope. Hence, TtHBDH enables the asymmetric reduction of methyl β-ketoesters, while LkKRED provides access to β-ketoesters with bulkier substituents at the alpha and gamma-carbon.
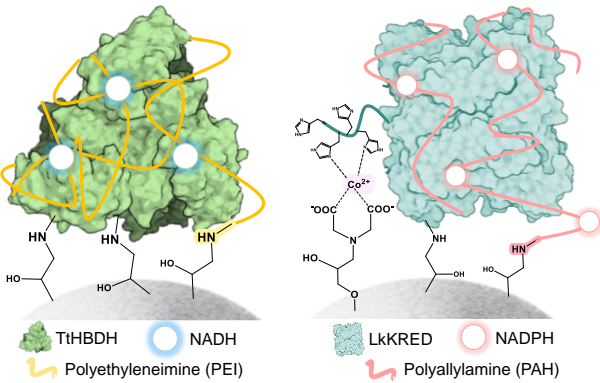
Fabrication of self-sufficient heterogeneous biocatalysts

After characterizing the kinetic parameters of these two enzymes across a variety of substrates, we next co-immobilised them with their respective redox cofactors to fabricate a self-sufficient heterogeneous biocatalyst (ssHB). Using ssHBs, we only need to add the substrate and the sacrificial co-substrate for cofactor regeneration to steer the process. Despite the absence of a universal method for all enzymes, ssHB construction usually involves three steps: immobilizing the enzyme on a solid support, coating the immobilised enzyme with a cationic polymer, and co-immobilizing the cofactor (**Figure S3**).

For the enantioselective production of (*S*)-β-hydroxyacids, our group has already developed an active and robust ssHB based on the NADH-dependent TtHBDH immobilised on agarose beads functionalised with glyoxyl groups (AG-G) and coated with branched polyethyleneimine (PEI).[41] Hereinafter, this ssHB is dubbed as TtHBDH@ssHB. Following the same protocol, we prepared a ssHB based on the NADPH-dependent His-tagged LkKRED to access (*R*)-β-hydroxy esters. LkKRED was active upon its immobilization on AG-G but its storage stability was extremely low (**Figure S4**). Alternatively, we immobilised this enzyme on agarose beads activated with cobalt chelates and epoxy groups (AG-Co^{2+}/E). The immobilisation relies on the selective interaction between the His-tag and the cobalt chelates of the support, enabling the enzyme orientation through its N-terminus where the His-tag is fused. Moreover, this

immobilisation procedure allows the one-step purification and immobilisation of the enzyme from crude lysates, retaining its initial activity upon 24 hours of incubation at 4º C (**Figure S4**). Hence, we selected (AG-Co^{2+}/E) to assemble the ssHB. Next, we coated this immobilised LkKRED with either PEI or Polyallylamine (PAH) as cationic polymers to further immobilise the redox cofactor (NADPH).[36] We found that the PEI coating reduced the activity of the immobilised enzyme by $> 90\%$, while the enzyme activity was negligibly affected after PAH coating (**Figure S5**). The higher activity retention upon polymer coating when comparing PAH with PEI has also been observed for the alcohol dehydrogenase from *Bacillus stearothermophilus* immobilised on AG-Co^{2+}/E.[36] In light of these results, we selected AG-Co^{2+}/E as support and PAH as a polymer to assemble an *R*-selective ssHB based on His-tagged LkKRED. Hereinafter, this ssHB is dubbed as LkKRED@ssHB.

Table 2. Scheme of TtHBDH and LkKRED ssHB and immobilisation and kinetic parameters towards 1a

	TtHBDH	NADH
	Polyethyleneimine (PEI)	
	LkKRED	NADPH
	Polyallylamine (PAH)	

	Enzyme		TtHBDH	LkKRED
	Carrier Chem.		Agarose Glioxil	Agarose Co^{2+}/Epoxy
Enzyme Immobilisation	Load[a]	mg g^{-1}	25,6	25,1
	Yield[b]	%	93,1	77,3
	rA[c]	U g^{-1}	0,84 ± 0,05	0,67 ± 0,10
	isA[d]	U mg^{-1}	0,032 ± 0,002	0,026 ± 0,001
Cofactor Immobilisation	NAD(P)H[e]	µmol g^{-1}	6,54	8,1
Kinetic Parameters Of ssHB	$V_{max\ app}$	U mg^{-1}	0,082 ± 0,005	0,051 ± 0,006
	$K_{M\ app}$	mM	66 ± 8	7,0 ± 2,9
	$k_{cat\ app}$	s^{-1}	0,26 ± 0,02	0,20 ± 0,02
	$k_{i\ app}$	mM	584 ± 78	419 ± 139
	k_{cat}/K_M	mM^{-1} s^{-1}	0,004 ± 0,002	0,028 ± 0,008

Table 2. Scheme of TtHBDH and LkKRED Self-Sufficient Heterogeneous Biocatalyst. Experimental protocols and parameter calculations are described in materials and methods section. a) Offered mg of enzyme per g of carrier. b) Protein immobilisation yield c) Recovered activity upon enzyme immobilisation. d) Specific activity at 30 ºC of immobilised enzyme and Relative activity regarding the specific activity of free enzymes (TtHBDH = 0.12 U mg^{-1}; LkKRED = 1.18 U mg^{-1}). e) µmol of NADH or NADPH per g of ssHB (offered 10 µmol g^{-1}) Kinetics of free enzymes in Table 1 (1a)

After establishing the optimal protocols for the fabrication of ssHBs, we maximised their protein loading and characterised the immobilisation process and the kinetics of the resulting ssHBs. **Table 2** shows the immobilisation and apparent kinetic (K_M and k_{cat}) parameters after offering concentrated crude and partially purified extracts of LkKRED and TtHBDH, respectively, to their respective carriers. We achieved an immobilisation yield >75% for both enzymes, giving raise to heterogeneous biocatalysts with similar volumetric and specific activities. Regarding the cofactor load, PEI coating in TtHBDH@ssHB immobilised 6,5 µmol$_{NADH}$ g^{-1}, while PAH coating of LkKRED@ssHB

11

loaded 8,1 μmol_{NADPH} g^{-1}. This result matches with previous results reported for other ssHBs.[36, 41]

To further investigate the kinetic behaviour of both ssHBs, we evaluated their initial rates under different substrate concentrations, using **1a** as the model substrate (**Figure S6**). These experiments allowed us to calculate the apparent Michaelis-Menten parameters for each immobilised enzyme, including the substrate inhibition constant where applicable. Upon immobilisation, both LkKRED@ssHB and TtHBDH@ssHB exhibited lower $^{app}k_{cat}$ values (83-fold and 25-fold lower, respectively) compared to their soluble enzymes. However, the $^{app}k_{cat}$ values for both ssHBs fall in a similar range, consistent with the specific activity of the immobilised enzymes reported above (**Table 2**). Regarding the changes in $^{app}K_M$ after immobilisation, TtHBDH exhibited a decrease of 11.2, whereas LkKRED showed an increase by a factor of 37. The presence of different polymeric coatings may introduce additional complexities that influence the apparent constants. With the PAH coating, higher substrate concentrations seem to be required to increase the local concentrations within the bead where LkKRED is immobilised, resulting in increased $^{app}K_M$ and Ki (2.7-fold) compared to soluble enzymes. This suggests the presence of mass transfer limitations and reduced substrate accessibility. On the other hand, the PEI coating showed different effects on TtHBDH, including lower $^{app}K_M$ values and the occurrence of substrate inhibition, which was not observed for soluble enzymes. This indicates that the PEI coating may affect substrate binding or alter the enzyme microenvironment, resulting in different catalytic behaviour. Overall, changes in $^{app}K_M$ during immobilisation can be influenced by numerous factors, including mass transfer limitations, substrate-support interactions, and may vary between different enzymes and immobilisation strategies. Our findings are supported by previous reports where $^{app}K_M$ can either increase or decrease compared to the free enzyme, depending on the factors

12

mentioned above.[43-45] We suggest that a combination of these factors leads to the significant decrease observed in the apparent catalytic efficiency. Nonetheless, we envision that future efforts to understand the role of immobilisation and polymeric coating in substrate diffusion limitations, K_M value, and consequently the production of these biocatalysts will approach the industrial demands.

To validate the self-sufficiency of LkKRED@ssHB and confirm its enantioselectivity for the *R* configuration, we analysed the reaction progress for the reduction of **1a** with cofactor regeneration using isopropanol as ancillary substrate **(Figure S7A-B)**. LkKRED@ssHB completed the conversion of 200mM **1a** to **2a** in less than 5 hours at 25 ºC in 1 mL batch reactions **(Figure S7A-B)**. In contrast, TtHBDH@ssHB only achieved 89% conversion in 24 h under the same conditions.[41] Only when the temperature was raised to 60ºC, TtHBDH@ssHB exhibited similar batch productivity to that of LkKRED@ssHB at 25ºC.[41] Therefore, the higher catalytic efficiency of LkKRED@ssHB is reflected in higher operational productivity to that of TtHBDH@ssHB. We also tested the reaction using 1 M **1a** and 10% (*v/v*) isopropanol reaching a 77 % chromatographic product yield (CY) in 72h, which meant a specific productivity 3,7 times lower than using 200 mM substrate concentration **(Figure S7B)**. The lower volumetric productivity at higher substrate loads is explained by the substrate inhibition undergone by LkKRED as supported by its kinetic data (**Tables 1** and **2)**. Next, we analysed the stereo configuration of the reaction product by GC-FID chiral analysis **(Figure S7C)**, confirming the exquisite *R*-selectivity of the immobilised biocatalyst, which yielded ethyl (*R*)-3-hydroxybutyrate with *ee* > 99%, indicating that the immobilisation process maintains the enzyme enantioselectivity.

13

Optimisation of continuous flow operation

Once we had two active ssHBs to asymmetrically reduce β-keto esters with excellent divergent enantioselectivities, we packed them into two different packed bed reactors (PBR). We first performed the continuous biosynthesis of **(S)-2a** at 50 ºC with a PBR loaded with 1 g TtHBDH@ssHB (25,6 mg_{TtHBDH} g^{-1}, V_R: 1.4 mL) coupled to an in-line spectrophotometer to monitor the cofactor lixiviation at the reactor outlet. Temperature was increased owing to the thermophilic nature of TtHBDH to ultimately aim at enhancing biocatalyst productivity. To evaluate the PBR performance, we tested a range of flow rates (0,01-0,2 mL min-1) and substrate (**1a**) concentrations (50 to 1000 mM) using isopropanol in 10 mM Tris-HCl buffer at pH 7 (**Figure 2A**). The substrate conversion and product yield were determined by GC-FID to calculate the Space-Time Yield (STY) and chromatographic yield (CY). **Figure 2B** shows an inverse linear correlation between CY and the STY when flow rates are increased in the 50-200 mM **1a** range, leading to lower CYs at higher STYs. However, the PBR operated with 1 M **1a** unfollows this trend since the maximum STY(150 g L^{-1} h^{-1}) reached at the highest flow rate (0.2 mL min^{-1}) gives rise to the second highest CY (35%). Based on STY and CY data for each operation condition, we established a threshold for the optimal PBR (V = 1.4 mL) operation setting a minimum of CY ≥ 80% and STY ≥ 30 g L^{-1} h^{-1} of STY. According to this threshold, we select a flow rate of 0.05 mL min^{-1} with a 200 mM substrate (**1a**) to operate the *S*-selective PBR with the optimal STY-CY balance. Under these conditions, we also monitored the NADH lixiviation continuously, detecting negligible amounts of NADH at the reactor outlet (**Figure S8**).

Guided by the results achieved with the (*S*)-selective PBR, we next performed the continuous biosynthesis of **(R)-2a**. Unlike TtHBDH, the mesophilic nature of LkKRED enables us to achieve significant CY levels at a lower temperature (25 ºC). The PBR was

14

loaded with 0.5 g of LkKRED @ssHB (25.1 mg_{TtHBDH} g^{-1} V_R: 0.7 mL). Due to LkKRED@ssHB exhibiting a catalytic efficiency 7-fold higher than TtHBDH@ssHB (**Table 2**), we set up a reactor with half of the volume (half biocatalyst mass) to operate in the same flow range and determine the productivity boundaries of the immobilised LkKRED under the tested conditions. Using 200mM **1a**, we performed a flow rate ramp for this PBR to find the optimal conditions that maximise the CY-STY balance of (**R**)-**2a**. Like the (S)-selective PBR based on TtHBDH@ssHB, this (R)-selective PBR also achieves its optimal CY-STY balance at 0.05 mL min^{-1}, estimating a CY = 100% and a maximum STY of 55 g L^{-1} h^{-1} for a PBR loaded with 1 g (1.4 mL) LkKRED@ssHB.
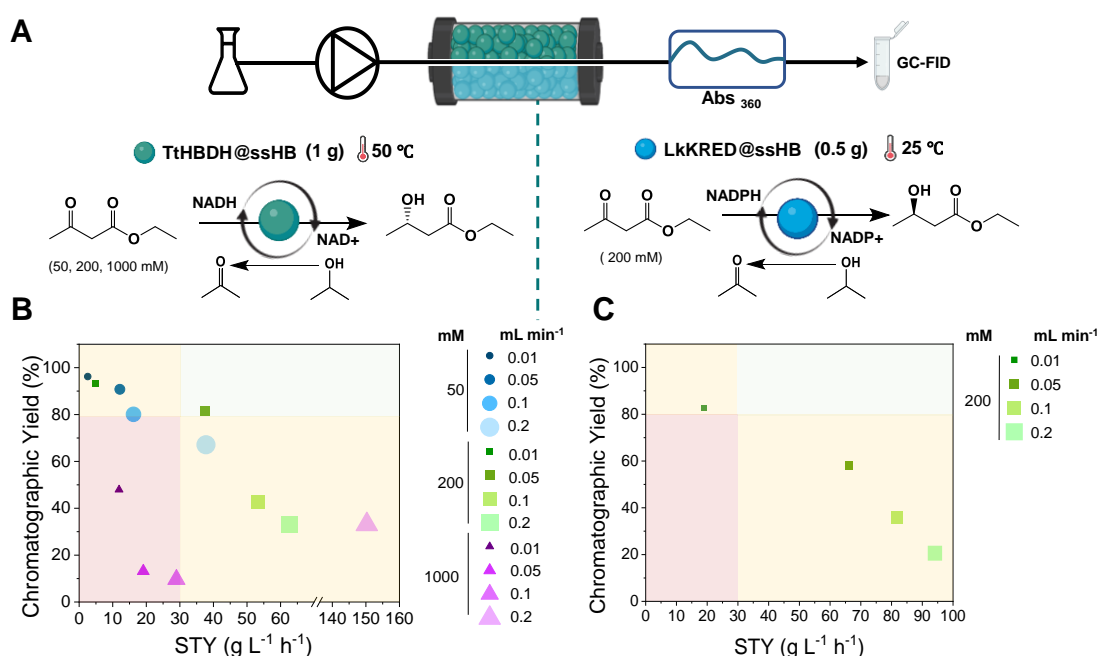
Figure 2: A) Scheme of continuous flow reaction with PBRs packed with TtHBDH@ssHB and LkKRED@ssHB. Chromatographic Yield (%) vs Space-Time Yield ($g_{product}$ L^{-1} h^{-1}) obtained at the different conditions of flow rate and substrate concentration evaluated in continuous operation with a S- and R- selective PBRs loaded with TtHBDH@ssHB (B) and LkKRED @ssHB (C) at 50 and 25° C, respectively.

To better understand the bottlenecks these two enantiodivergent PBRs face during their continuous operation, we simulated their performances in batch and flow using the kinetic parameters reported in **Table 2**. The simulation of the batch reactor only converges with the experimental data if product and substrate inhibitions are considered in the reactor kinetic equation (see supporting information, **Figure S9**). The product inhibition constant estimated for LkKRED@ssHB is 3.9 times lower than that estimated for TtHBDH@ssHB (**Table S2**). To experimentally prove the occurrence of product inhibition, we incubated both ssHBs at different product (*R*)- or (*S*)-**2a** concentrations (10-500 mM) and quantified their specific reaction rates. The experiments confirmed the existence of product inhibition in both ssHBs (**Figure S10**). Thus, simulated parameters allow the evaluation of inhibition constants, providing valuable insights for process optimisation and control. If the performance of the flow reactor is ideal, its experimental values should match those obtained from the batch reactor when the CY is plotted as a function of the dimensionless reaction time. However, neither was the case with TtHBDH@ssHB nor LkKRED@ssHB (**Figure S9**). This deviation from ideality was more notorious at low flow rates (high dimensionless reaction time) and with the more productive enzyme (LkKRED). To explain this fact, we incorporated the axial flow dispersion within the PBRs into the kinetic model, achieving an excellent fitting of the experimental data for all tested flow rates (**Figure S9**). According to these simulations, both PBRs only perform ideally when the dimensionless reaction time is lower than 2.5 using 200 mM **1a**, supporting the fact that 0.05 mL min^{-1} is the optimal flow rate to maximise the CY-STY balance.

Long-term operational stability of TtHBDH and LkKRED ssHB

Once the two enantiodivergent PBRs were kinetically characterised, we studied their long-term operational stability by continuously feeding freshly prepared PBRs (1g of ssHB, V_R: 1.4 mL) with 200 mM **1a** at 0.05 mL min^{-1}. Surprisingly, the PBR loading the

16

less thermostable enzyme (LkKRED) was significantly more stable under its corresponding operation conditions than the most thermostable one. (S)-selective PBR loaded with TtHBDH@ssHB reached a transient CY > 95% after 2 h, yet its catalytic activity dramatically decayed along the time which reduced CY below 50% after 48 h operation. This enzyme inactivation means that STY decreases from 49 to 27 g L^{-1} h^{-1}. During this time, a total volume of 144 mL was processed, yielding an accumulated Total Turnover Number (TTN) of TtHBDH and NADH of 1.46 x 10^5 and 2984, respectively (**Figure 3A**). The TTN of TtHBDH is more than 4.5 times higher than the previously reported with other thermophilic dehydrogenases.[38, 39]

In contrast, the (R)-selective PBR loaded with LkKRED@ssHB maintained a CY between 90.2 % to 46 % during 21 days of continuous operation without an exogenous supply of NADPH. As a result, STY only ranged from 49.5 to 25.3 g L^{-1} h^{-1} in that operational time frame, collecting a total volume of 1500 mL. Remarkably, the LkKRED@ssHB reaches an accumulated TTN 9.37 x 10^5 and 27240 for the enzyme and NADPH, respectively (**Figure 3B**). Although both PBRs exhibit similar STYs at the early operation, the high accumulated TTN values for both enzyme and cofactor make LkKRED@ssHB more productive and more robust than TtHBDH@ssHB when they operate at 30 and 50 ℃, respectively.

The synthesis of both (***R***) and (***S***)-**2a** using PBRs are accomplished with higher STY than similar ssHBs operated for the asymmetric oxidation of secondary alcohols in flow[39], and in the same range as those STYs reported for gram scale biosynthesis of (S)-**2e** using whole-cell biocatalysts in aqueous media[45] and biphasic systems.[46]
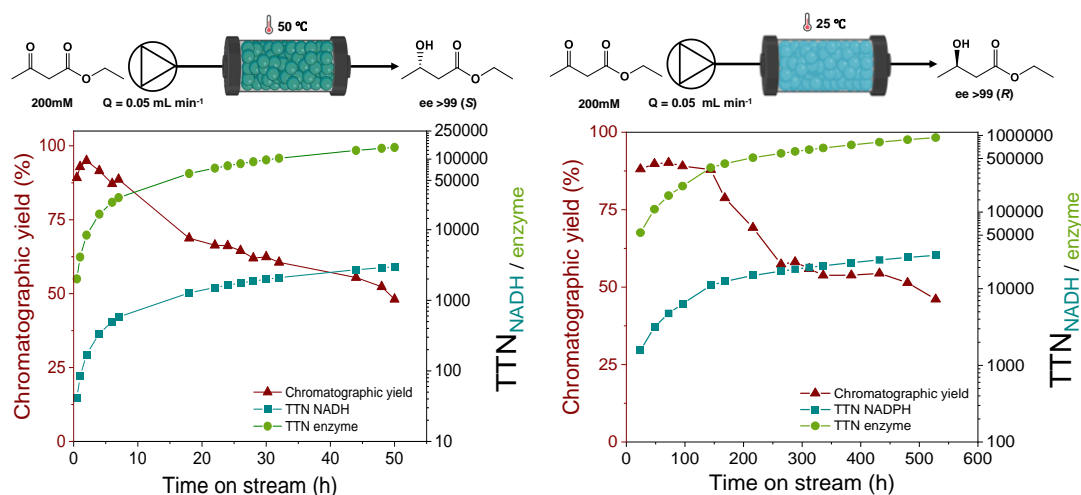
Figure 3 Continuous flow long-term operation set-up and plot of Conversion vs TTN of enzyme and cofactor of A) TtHBDH@ssHB or B) LkKRED@ssHB in the reduction of 200mM of **1a**.

Unveiling the causes behind the operational inactivation of TtHBDH@ssHB

To understand the reasons behind the conversion decay observed with the most thermostable ssHB during long-term operation, we conducted *ex-situ* post-used and *in situ* operando analysis of TtHBDH@ssHB under the operation conditions we described above (200 mM 1a, 0.5 mL min^{-1} and 50 °C). First, we unpacked the PBR and withdrew samples of ssHB from three PBR zones (inlet, medium, and outlet) to characterise the enzyme exhaustion and cofactor unload. The TtHBDH activity after 48 hours of operation only decreased by 10% compared to samples incubated with fresh reaction media including cofactor, suggesting that the 50% CY decay must be explained by other factors rather than enzyme inactivation (**Figure 4A**).

18
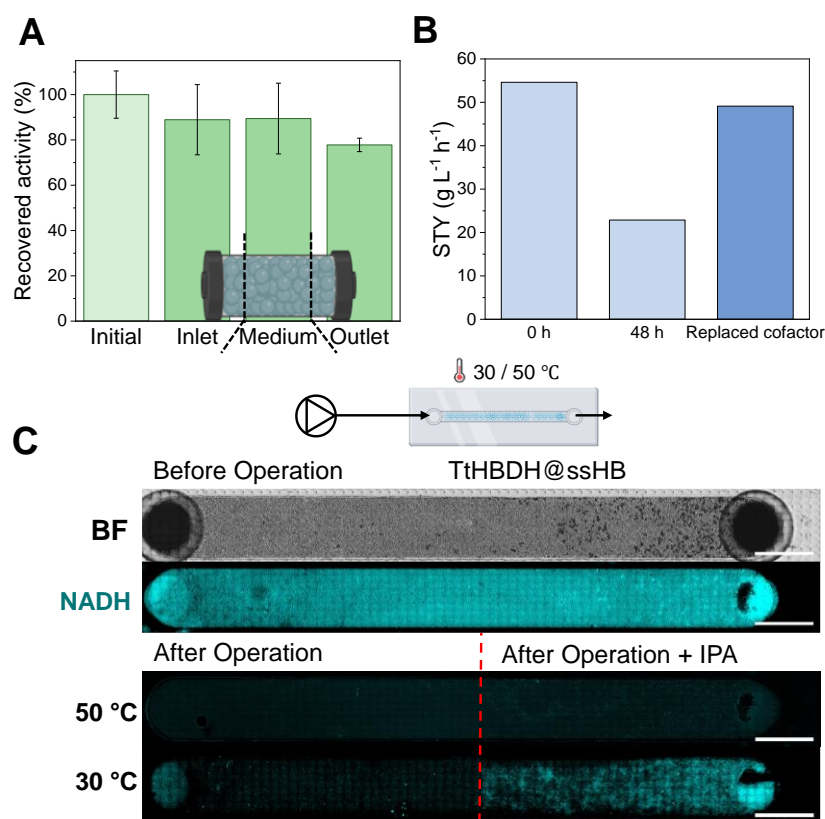
Figure 4: A) Recovered activity of TtHBDH@ssHB in different sections of the PBR before and after 48h operation at 50 ºC. B) Productivity recovery after NADH replacement in TtHBDH@ssHB C) TtHBDH@ssHB packed bed slide reactor in BF and DAPI channels before and after 24h operation at 30 or 50 °C in the reduction of 200mM of 1a. The post-operation NADH stability was analysed by flushing a solution of 5% isopropanol to study its regeneration.

To explore other inactivation causes related to the immobilised cofactor, first, we extracted any residual cofactor from the TtHBDH@ssHB by incubating it with 1 M NaCl, then the same immobilisate was incubated with freshly prepared NADH for 1 hour. This reloaded ssHB was re-packed again into the PBR and operated at 50º C to determine the STY. **Figure 4B** shows that STY of TtHBDH@ssHB was restored to its initial value, suggesting that either the cofactor was lixiviated along operation, or it was chemically degraded due to the high operational temperature. Since we already demonstrated that

19

NADH was not lixiviated during the process (**Figure S8**), we hypothesise that NADH suffers bond breakage triggered by the process temperature. To determine this degradation, we eluted the cofactor from the operated TtHBDH@ssHB by incubating it with 1 M NaCl, and analysed the eluted fraction by UPLC-MS. As a result, we detected a NAD^+ degradation fragment of 414 Da but neither we did NADH nor NAD^+ (**Figure S11**). This insight supports that the redox cofactor was retained within ssHB in its oxidised form (NAD^+) but was chemically degraded during the operation process, explaining the decay in the STY found for this PBR. This thermal degradation of NAD(P)H agrees with the fragmentation of this cofactor previously reported at high temperatures.[47]

To support the temperature-driven decomposition of the immobilised redox cofactor under operation conditions, we replicated the PBR setup using a channel slide with a volume of 100 μL to monitor the cofactor fate through monitoring its autofluorescence during the continuous process. The slide reactors containing TtHBDH@ssHB were operated at two different temperatures (30 and 50º C) for 24h. Consistent with previous findings, the intraparticle fluorescence of NADH decreases during the operation span, indicating that the cofactor predominantly exists in its oxidised form, which is non-fluorescent. Then, the reaction was stopped, and only isopropanol was flushed to regenerate the NADH. Upon observation under the microscope, we found that only the reactor operated at 30°C increased its fluorescence, demonstrating the NADH regeneration. In contrast, the reactor operated at 50°C did not exhibit such regeneration. This observation suggests that temperature plays a significant role in the decomposition of NADH, as depicted in **Figure 4C**, preventing its regeneration, and causing a premature decrease in the product yield.

In light of these results, we suggest that LkKRED@ssHB exhibits greater operational stability than TtHBDH@ssHB because the former operates at 20 ℃ less than the latter, despite the higher thermal stability of TtHBDH compared to LkKRED. Thus, the thermophilic nature of TtHBDH can be seen as a double-edged sword in this context. While it imparts robustness to the enzyme, it also necessitates higher reaction temperatures (50-80°C) to operate at high rates where the co-immobilised cofactor is thermally degraded, causing the exhaustion of the PBR. This implies the necessity for careful evaluation when choosing thermophilic enzymes for extended process applications involving cofactors .

When we conducted operation at 25 ℃ for 21 days, the period required for a 50% reduction in CY during reaction extended from 2 to over 9 days. However, the CY achieved was 8.6 times lower than that at 50 ℃ (Figure S12). Subsequent attempts to purify the product by diethyl ether extraction from the reaction crude resulted in a 60% isolated yield, with the initial product still present (Figure S13).

Evaluation of process metrics

Encouraged by the excellent productivity and the operational stability results we achieved with both enantiodivergent PBRs, we made a comparison study with other self-sufficient heterogeneous biocatalyst reported in the literature. To that aim, we plot the accumulated TTN for both enzyme and cofactor as a function of the STY. This comparison study presented challenges due to the limited number of ssHBs reported in the literature, as well as the absence of certain metrics necessary for our analysis in some articles. In cases where these metrics were not explicitly provided, we made efforts to calculate them using available experimental data, providing the raw data in **Table S3**.

21
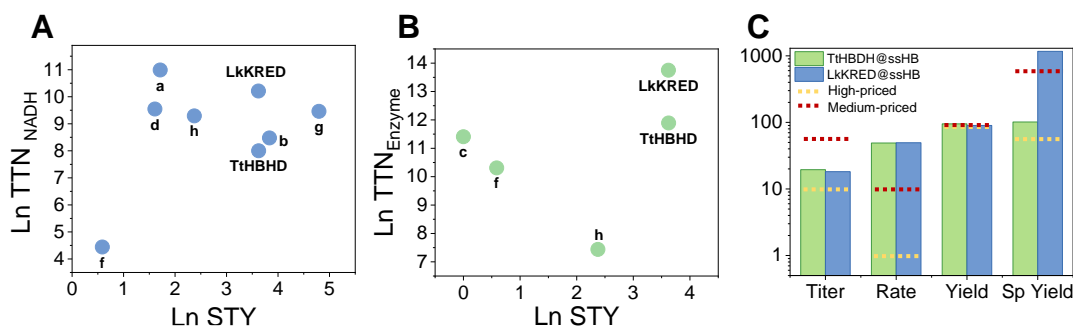
Figure 5: A) Ln of TTN_{enzyme} and B) Ln of $TTN_{NADH(P)H}$ as a function of Ln of STY resulted from the continuous operation of TtHBDH@ssHB and LkKRED@ssHB compared with other ssHBs already reported in the literature and operated in flow. Each letter corresponds to the literature references as follows; a[33]; b[48]; c[49]; d[50]; e[51]; f[38]; g[34]; h[52]. C): Mass metrics (Titre (g L^{-1}); Rate (g L^{-1} h^{-1}); Yield (%); Sp Yield (g gprotein^{-1})) of our processes compared with the range of mass-metrics proposed by Meissner and Woodley[53] for medium-(red, 5-100 \$ kg^{-1}) and high (orange, > 100 \$ kg^{-1}.)-priced products.

In the reduction of **1a** to (*R*)- and (*S*)-**2a,** both ssHBs display accumulated TTN values among the highest reported for cofactors and enzymes working in bioredox cascades. **Figure 5A** shows that the two enantiodivergent PBRs loaded with our LkKRED@ssHB and TtHBDH@ssHB exhibit a similar $TTN_{NAD(P)H}$-STY balance as the most robust self-sufficient heterogeneous biocatalysts reported till today. To the best of our knowledge, LkKRED@ssHB is only surpassed by one example reported by Baumer et al. (g)[34] where the synthesis of (*S*)-**2e** is described in a close-loop cofactor recycling system based on liquid-liquid extraction of the product with organic solvents.   TtHBDH@ssHB $TTN_{NAD(P)H}$-STY balance is near to those reported by Chen et al. (b)[48] in the asymmetric reduction of secondary ketones by crude enzyme hydrogels in continuous flow. When

22

focusing specifically on the TTN of NAD(P)H, the work of Wei et al.(a)[33] stands out as they reported the highest TTN number among self-sufficient biotransformations where exogenous cofactor is not supplied. In their study, they synthesised secondary alcohols in organic media by encapsulating a KRED with its respective cofactor in a Pickering emulsion, enhancing the cofactor reuse but with lower STY than LkKRED@ssHB and TtHBDH@ssHB. Regarding the enzyme accumulated TTN, our study reports the highest values for self-sufficient systems in continuous flow and among the highest found in flow biocatalysis using different non-cofactor dependent enzymes (i.e. hydrolases).[54]

Furthermore, we assessed the mass metrics of the two enantiodivergent PBRs for the biosynthesis of enantiomerically pure **2a** driven by either TtHBDH@ssHB or LkKRED@ssHB according to the parameters described by Meissner and Woodley.[53] **Figure 5C** illustrates how all the metrics achieved with both ssHBs fall between the lower limit between medium (5-100 \$ kg^{-1})- and high-priced ($>$ 100 \$ kg^{-1}) products according to the mass metrics proposed by Meissner and Woodley to manufacture chemicals. Remarkably, these ssHBs surpass the maximum range established for process rate and yield mass metrics for medium-priced products. As enantiomerically pure β-hydroxy esters may be considered between high-and medium-priced products, we emphasize the industrial potential of these two ssHBs.

Finally, we assessed the sustainability of the process by calculating the E factor for the continuous process using both PBRs (**Table S4**). In both processes performed with the two PBRs, the E factor is lower than 60 for both processes, falling in the range of the E factor demanded by fine chemicals industries, which is the sector that manufactures ethyl 3-hydroxy butyl esters. To note, water is the major contributing waste to the E-factor (**Figure S14**) in agreement with sustainability assessment of most biocatalytic processes reported in the literature.[55]

23

CONCLUSION

In summary, we have successfully developed two enantiodivergent self-sufficient heterogeneous biocatalysts (ssHBs) for the continuous asymmetric reduction of β-keto esters to their corresponding β-hydroxy esters. The substrate scope of one thermophilic dehydrogenase (TtHBDH) and mesophilic ketoreductase (LkKRED) support the versatility of these heterogeneous biocatalysts to access a variety of β-hydroxy esters with different substituents in alpha and gamma carbons. Through the optimisation of the immobilisation protocol, we managed to fabricate two robust, highly productive ssHBs with complementary enantioselectivities that meet the industrial cost standards for manufacturing fine chemicals. Furthermore, we investigated the unexpected exhaustion of the thermophilic TtHBDH@ssHB through ex-situ and operando studies. Herein, we unveil the chemical degradation of NADH at high temperatures as the main reason that explains the premature biocatalyst inactivation. Therefore, the temperatures required to efficiently exploit thermophilic enzymes *in vitro* can jeopardise the stability of the immobilised cofactors, demanding a conscientious pondering and optimisation to strike the activity-stability balance of ssHB considering the cofactor preservation. Hence, operating at low/moderate temperatures offers a solution to one of the major drawbacks of the application of oxidoreductases in chemical manufacturing, the cost of enzymes and cofactors. In essence, the development of robust and self-sufficient biocatalysts allows for reducing the NAD(P)H costs in the manufacturing of alcohols. In this case, based on the experimental data reported in **Figure 3C**, we estimate that the NADPH net cost per gram of product decreases from 200 € g^{-1} in a stoichiometric process to less than 0.04 € g^{-1} for the continuous synthesis ethyl 3-(*R*)-hydroxybutyrate using our self-sufficient heterogeneous biocatalysts.

Therefore, the development of ssHB in porous materials thus enables a straightforward, accessible, and cost-efficient technology that can be readily adapted to various single and multienzyme systems dependent on expensive cofactors. This approach also holds potential not only for the pharmaceuticals industry but also for fine chemistry industries where biocatalysis can be employed in processes with tighter cost margins (food and cosmetic industries). Further investigation is necessary to explore the feasibility of expanding this system to accommodate additional enzymes and to understand the differences in behaviour induced by the action of the polymeric coating on both enzyme kinetics and stability.[56]

AUTHOR CONTRIBUTIONS

Experiments were performed by AM and DAS. Computational simulations were performed by JMB. The manuscript was written by DAS and FLG. The work was conceptualised by FLG. Funding was secured by FLG. All authors discussed the results and revised the manuscript. All authors have given approval to the final version of the present manuscript.

ASSOCIATED CONTENT

Supporting Information. Materials and Methods and experimental results are shown as supporting Figures and Tables including synthetic protocols of the substrates, modelling protocols, the Michaelis-Menten plots and other relevant information to support the result shown in the main manuscript.

CONFLICT OF INTEREST

There are no conflicts to declare.

ACKNOWLEDGMENTS

REFERENCES

1. *S. Christopher, Enzymatic processes for the production of 4-substituted 3-hydroxybutyric acid derivatives and vicinal cyano, hydroxy substituted carboxylic acid esters,* 2004.
2. J. Zhang, Q. Cao, S. Li, X. Lu, Y. Zhao, J.-S. Guan, J.-C. Chen, Q. Wu and G.-Q. Chen, *Biomaterials*, 2013, **34**, 7552-7562.
3. X.-H. Zou, H.-M. Li, S. Wang, M. Leski, Y.-C. Yao, X.-D. Yang, Q.-J. Huang and G.-Q. Chen, *Biomaterials*, 2009, **30**, 1532-1541.
4. K. Mori, *Tetrahedron*, 1989, **45**, 3233-3298.
5. R. N. Patel, *Biomolecules*, 2013, **3**, 741-777.
6. L. Chai, H. Chen, Z. Li, Q. Wang and F. Tao, *Synlett*, 2006, **2006**, 2395-2398.
7. A. I. Meyers and R. A. Amos, *J. Am. Chem. Soc.*, 1980, **102**, 870-872.
8. H. Dong, S. Liffland, M. A. Hillmyer and M. C. Y. Chang, *J. Am. Chem. Soc.*, 2019, **141**, 16877-16883.
9. K. y. R. Bannister and K. L. J. Prather, *Curr. Opin. Biotechnol.*, 2023, **79**, 102852.
10. A. E. Díaz-Alvarez, L. Mesas-Sánchez and P. Dinér, *Molecules*, 2014, **19**, 14273-14291.
11. G. Solladié, C. Bauder, E. Arce-Dubois and Y. Pasturel-Jacopé, *Tetrahedron Lett.*, 2001, **42**, 2923-2925.
12. M. Braun, *Angew. Chem. Int. Ed.*, 1987, **26**, 24-37.
13. P. V. Ramachandran and P. B. Chanda, *Org. Lett.*, 2012, **14**, 4346-4349.
14. A. Mi, Z. Wang, J. Zhang and Y. Jiang, *Synth. Commun.*, 1997, **27**, 1469-1473.
15. L. Ouyang, Y. Xia, Y. Wei, J. Liao and R. Luo, *ACS Omega*, 2020, **5**, 16967-16975.
16. P. G. Cozzi, *Angew. Chem. Int. Ed.*, 2006, **45**, 2951-2954.
17. R. Noyori, T. Ohkuma, M. Kitamura, H. Takaya, N. Sayo, H. Kumobayashi and S. Akutagawa, *J. Am. Chem. Soc.*, 1987, **109**, 5856-5858.
18. M. A. Ariger and E. M. Carreira, *Org. Lett.*, 2012, **14**, 4522-4524.
19. B. Wipf, E. Kupfer, R. Bertazzi and H. G. W. Leuenberger, *Helv. Chim. Acta*, 1983, **66**, 485-488.
20. M. North, *Tetrahedron Lett.*, 1996, **37**, 1699-1702.
21. J.-Y. He, L.-M. Zhou, P. Wang and L. Zu, *Process Biochem.*, 2009, **44**, 316-321.
22. M. Cvjetko Bubalo, M. Mazur, K. Radošević and I. Radojčić Redovniković, *Process Biochem.*, 2015, **50**, 1788-1792.
23. S. Rodríguez, M. M. Kayser and J. D. Stewart, *J. Am. Chem. Soc.*, 2001, **123**, 1547-1555.

24. J. Kim, J. H. Chang, E.-J. Kim and K.-J. Kim, *Biochem. Biophys. Res. Commun.*, 2014, **443**, 783-788.
25. Z. Yang, W. Ye, Y. Xie, Q. Liu, R. Chen, H. Wang and D. Wei, *Org. Process Res. Dev.*, 2020, **24**, 1068-1076.
26. L. Yáñez, Y. Rodríguez, F. Scott, A. Vergara-Fernández and R. Muñoz, *Bioresour. Technol.*, 2022, **353**, 127141.
27. A. Dudzik, W. Snoch, P. Borowiecki, J. Opalinska-Piskorz, M. Witko, J. Heider and M. Szaleniec, *Appl. Microbiol. Biotechnol.*, 2015, **99**, 5055-5069.
28. S. Shimizu, M. Kataoka, M. Katoh, T. Morikawa, T. Miyoshi and H. Yamada, *Appl. Environ. Microbiol.*, 1990, **56**, 2374-2377.
29. J. Son, H. Lee, T. Lee, H. Sohn, S. Jae Park, J.-G. Na, S. Woo Seo, J. Wook Lee, H. Young Yoo and C. Park, *J. Ind. Eng. Chem.*, 2023, **123**, 355-360.
30. J. M. Bolivar, J. M. Woodley and R. Fernandez-Lafuente, *Chem. Soc. Rev.*, 2022, **51**, 6251-6290.
31. R. A. Rocha, A. J. North, R. E. Speight, C. C. Williams and C. Scott, *Catalysts*, 2022, **12**, 1454.
32. K. Seelbach and U. Kragl, *Enzyme Microb. Technol.*, 1997, **20**, 389-392.
33. W. Wei, R. Ettelaie, X. Zhang, M. Fan, Y. Dong, Z. Li and H. Yang, *Angew. Chem. Int. Ed.*, 2022, **61**, e202211912.
34. B. Baumer, T. Classen, M. Pohl and J. Pietruszka, *Adv. Synth. Catal.*, 2020, **362**, 2894-2901.
35. F. López-Gallego, G. Fernandez-Lorente, J. Rocha-Martin, J. M. Bolivar, C. Mateo and J. M. Guisan, *Methods Mol. Biol.*, 2013, **1051**, 59-71.
36. E. Diamanti, J. Santiago-Arcos, D. Grajales-Hernández, N. Czarnievicz, N. Comino, I. Llarena, D. Di Silvio, A. L. Cortajarena and F. López-Gallego, *ACS Catal.*, 2021, **11**, 15051-15067.
37. A. I. Benítez-Mateos, E. San Sebastian, N. Ríos-Lombardía, F. Morís, J. González-Sabín and F. López-Gallego, *Chem. Eur. J.*, 2017, **23**, 16843-16852.
38. S. Velasco-Lozano, A. I. Benítez-Mateos and F. López-Gallego, *Angew. Chem. Int. Ed.*, 2017, **56**, 771-775.
39. A. I. Benítez-Mateos, M. L. Contente, S. Velasco-Lozano, F. Paradisi and F. López-Gallego, *ACS Sustain. Chem. Eng.*, 2018, **6**, 13151-13159.
40. P. De Santis, L.-E. Meyer and S. Kara, *React. Chem. Eng.*, 2020, **5**, 2155-2184.
41. A. H. Orrego, D. Andrés-Sanz, S. Velasco-Lozano, M. Sanchez-Costa, J. Berenguer, J. M. Guisan, J. Rocha-Martin and F. López-Gallego, *Catal. Sci. Tech.*, 2021, **11**, 3217-3230.
42. A. Weckbecker and W. Hummel, *Biocatal. Biotransform.*, 2006, **24**, 380-389.
43. M. R. Khan, *Bull. Natl. Res. Cent.*, 2021, **45**, 207.
44. D. Feng, T.-F. Liu, J. Su, M. Bosch, Z. Wei, W. Wan, D. Yuan, Y.-P. Chen, X. Wang, K. Wang, X. Lian, Z.-Y. Gu, J. Park, X. Zou and H.-C. Zhou, *Nat. Comm.*, 2015, **6**, 5979.
45. S. Talekar and S. Chavare, *Recent Res. J. Sci. Technol*, 2012, **4(02)**, 01-05.
46. S. Shah, R. Agera, P. Sharma, A. V. Sunder, H. Singh, H. M. James, R. P. Gaikaiwari and P. P. Wangikar, *Process Biochem.*, 2018, **70**, 71-78.
47. D. Hofmann, A. Wirtz, B. Santiago-Schübel, U. Disko and M. Pohl, *Anal. Bioanal. Chem.*, 2010, **398**, 2803-2811.
48. Q. Chen, Y. Wang and G. Luo, *ChemSusChem*, 2023, **16**, e202201654.
49. H. A. Reeve, L. Lauterbach, O. Lenz and K. A. Vincent, *ChemCatChem*, 2015, **7**, 3480-3487.

50. T. Peschke, P. Bitterwolf, S. Gallus, Y. Hu, C. Oelschlaeger, N. Willenbacher, K. S. Rabe and C. M. Niemeyer, *Angew. Chem. Int. Ed.*, 2018, **57**, 17028-17032.
51. X. Ji, Z. Su, P. Wang, G. Ma and S. Zhang, *ACS Nano*, 2015, **9**, 4600-4610.
52. C. J. Hartley, C. C. Williams, J. A. Scoble, Q. I. Churches, A. North, N. G. French, T. Nebl, G. Coia, A. C. Warden, G. Simpson, A. R. Frazer, C. N. Jensen, N. J. Turner and C. Scott, *Nat. Catal.*, 2019, **2**, 1006-1015.
53. M. P. Meissner and J. M. Woodley, *Nat. Catal.*, 2022, **5**, 2-4.
54. J. M. Bolivar and F. López-Gallego, *Curr. Op. Green. Sustain. Chem.*, 2020, **25**, 100349.
55. R. A. Sheldon, *Green Chem.*, 2023, **25**, 1704-1728.
56. H. Sánchez-Morán, L. R. B. Gonçalves, D. K. Schwartz and J. L. Kaar, *ACS Catal.*, 2023, **13**, 4304-4315.

<u>Supporting information</u>

Enantiodivergent Synthesis of β-Hydroxy esters by Self-Sufficient Heterogeneous Biocatalyst in Continuous Flow.

Daniel Andrés-Sanz,[a] Ainhoa Maiz-Iginitz, [ab] Juan M. Bolivar[c], Alejandro H. Orrego,[a] Haritz Sardon,[b] and Fernando López-Gallego*[a,d]

a. *Heterogeneous Biocatalysis Laboratory, Center for Cooperative Research in Biomaterials (CIC biomaGUNE), Basque Research and Technology Alliance (BRTA), Paseo de Miramón 182, Donostia San Sebastián, Spain*

b. *POLYMAT and Department of Polymers and Advanced Materials: Physics, Chemistry and Technology, Faculty of Chemistry, University of the Basque Country UPV/EHU, Paseo Manuel de Lardizábal, 3, 20018 Donostia-San Sebastián, Spain*

c. *FQPIMA Group Department of Chemical Engineering, Complutense University of Madrid, Madrid, Spain*

d. *IKERBASQUE, Basque Foundation for Science, María Díaz de Haro 3, 48013 Bilbao, Spain*

*Corresponding author
Fernando López-Gallego: flopez@cicbiomagune.es

29

Contents

Materials and Methods

Materials.

Polyethyleneimine branched (PEI) (Mw ~25 kDa), polyallylamine (PAH) solution in

H_2O (Mw ~65 kDa, 10 wt.%), isopropanol, ethyl acetoacetate (1a), ethyl 2-

methylacetoacetate (1b); ethyl 2-ethylacetoacetate (1c); ethyl 2-chloroacetoacetate (1d);

ethyl 4-chloroacetoacetate (1e) iminodiacetic acid (IDA), and other reagents and

solvents of analytical grade were purchased from Sigma-Aldrich (St. Louis, IL, USA).

Agarose microbeads 6BCL (50-150 µm diameter) were purchased from Agarose Bead

Technologies (Madrid, Spain). Reduced Nicotinamide-adenine-dinucleotides sodium

salts (NAD(P)H) were purchased from GERBU Biotechnik GmbH (Heidelberg,

Germany). Bradford protein assay dye reagent was purchased from BIORAD (Bio-Rad.

Hercules, CA, USA) µ-Slides 8 well glass bottom was purchased from Ibidi (Planegg,

Germany).

Expression and purification of TtHBDH and LkKRED

The (*S*)-3-hydroxybutyryl-CoA dehydrogenase from *Thermus thermophilus* HB27

(TtHBDH) and the Ketoreductase from *Lactobacillus kefir* were expressed and purified,

as described elsewhere.[1, 2] Briefly, a pET28b plasmid encoding the corresponding

enzymes (Table S1) were transformed in BL21 (DE3) E. coli cells. Colonies were

picked and grown in LB medium containing kanamycin (30 µg mL^{-1}). When an optical

density of 0.6 was reached, 1 mM of Isopropyl-β-thiogalactopyranoside (IPTG) was

added to induce the protein expression. The induced cultures continued for 3 h at 37 °C

for TtHBDH or 12 h at 21°C for LkKRED, then the bacteria were harvested by

centrifugation. Next, We resuspended the cells in 25 mM phosphate buffer pH 7 for

TtHBDH and a complex buffer (100 mM Tris buffer, 200mM NaCl, 1 mM $MgCl_2$) at

32

pH 7 for LkKRED. We lysed the bacteria through sonication and the cell debris was discarded by centrifugation (10000 g for 15 min). For TtHBDH, the soluble crude protein extract was incubated at 70 °C for 45 min to purify the thermophilic enzyme through thermal shock, as previously described.[1] The pellets of denatured mesophilic proteins were discarded after centrifugation (10000 g for 30 min). For LkKRED the soluble crude protein extract was purified through immobilization with metal affinity chromatography using agarose microbeads.(ABT, Madrid, Spain) functionalized with Co^{2+} chelates. The protein was eluted with a solution of 100 mM Tris-HCl, 200 mM NaCl, 1 mM $MgCl_2$ and 500 mM imidazole at pH 7. The imidazole was removed from purified enzymes by gel filtration using a PD-10 column (GE Healthcare, Chicago, IL).

Determination of enzyme concentration.

The concentration of soluble enzymes (TtHBDH and LkKRED) was determined during the processes of purification and immobilization using the Bradford protein assay (Bio-Rad, CA). A standard curve was established using a commercial solution of bovine serum albumin (Sigma-Aldrich, St. Louis, IL). To measure the concentration, 5 µL of the soluble enzyme solution were combined with 200 µL of diluted Bradford reagent, and the mixture was incubated for 5 minutes at room temperature. The absorbance was then measured at 595 nm.

Enzyme activity Spectrophotometric assay

The enzymatic activities of soluble enzymes were determined in 96-well plates by monitoring the NAD(P)H absorbance at 340 nm. Five microliters of enzyme solution were incubated with 200 µL of a solution of 10 mM of 1a and 0.2 mM NAD(P)H in 25 mM phosphate buffer pH 7 at 30 °C. One enzyme unit (U) was defined as the amount of enzyme required to reduce 1 µmol of NAD(P)H per minute under given conditions and considering an $\varepsilon = 6.22$ mM^{-1} cm^{-1} for NADH at 340 nm

33

Synthesis of β-keto esters derivates

Concerning the synthesis of the substrates, meldrum acid (1r) and acyl chlorides (2r) were used as starting materials. Depending on the product needed, two different acyl chlorides were used, acetyl chloride or propionyl chloride (Reaction 1)
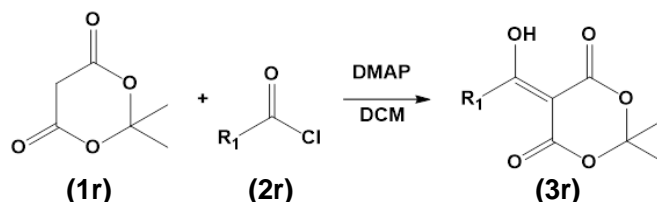
Reaction 1: Reaction between meldrum acid and acyl chloride.

In a 250 mL round-bottom flask equipped with a dropping funnel and under nitrogen atmosphere, meldrum acid (1 eq., 41.4 mmol) and 4-dimethylaminopyridine (DMAP) (2 eq., 82.2 mmol) were dissolved in 60 mL of anhydrous dichloromethane (DCM). The mixture was cooled down to 0 °C, and then the acyl chloride dissolved in 20 mL of anhydrous dichloromethane was added dropwise. The mixture was stirred for 24 hours at 25°C.

The reaction was quenched with 80 mL of 1M hydrochloric acid solution, observing that two phases were formed. The aqueous phase was extracted 2 times with dichloromethane. The organic phases were gathered, washed with 10 mL of NaCl saturated solution and dried over anhydrous Na_2SO_4. The solvent was removed in vacuo to yield the product (3r) as an orange solid, which was used for the next step without further purification (Reaction 2).
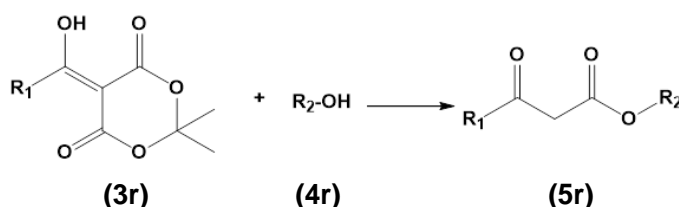

Reaction 2: Esterification of 3r.

In the second reaction, by adding the corresponding alcohol (4r) at appropriate temperature, an alcoholysis took place: under reflux the acyl meldrum (3r) was broken,

34

affording the corresponding β-keto ester (5r), as well as carbon dioxide and acetone as by-products. This reaction was done in a round-bottom flask equipped with a condenser. The compound 3r was dissolved in 100 mL of MeOH or EtOH and the reaction was constantly stirred for 16 hours and heated to reflux (for EtOH to 90 °C, for MeOH to 70 °C). Then the mixture was cooled down and the solvent removed under vacuo. The crude was purified by column chromatography (Hexane/Ethyl acetate: from 80:20 to 70:30) and the product was obtained as a pale yellow oil. Overall, the products showed in the Scheme 1S were obtained.[3, 4]
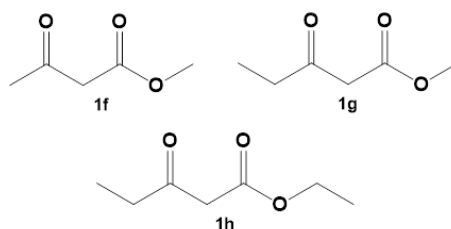
Scheme 1S: Obtained products from the synthesis.

The last synthesis was the addition of a methyl group on the α-carbon of the ethyl-3-oxopentanoate. The reaction showed in the Reaction 3, was the used procedure for the synthesis of both.
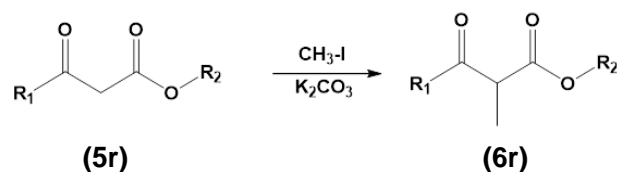

Reaction 3: Methylation in the α carbon.

For this reaction 5 g of the β-keto ester (5r) (1 eq., 38.4 mmol) were dissolved in 50 mL of anhydrous acetone under nitrogen atmosphere. Then, one equivalent of potassium carbonate (1 eq., 38.4 mmol), previously dried in the vacuum oven for 48 hours at 80 °C was added. The mixture was stirred for 15 minutes at room temperature. Afterwards

methyl iodide (1 eq., 38.4 mmol) was added. The reaction was stirred under reflux (75 °C) for 24 hours and checked by TLC.

For the extraction 60 mL of diethyl ether were added; the mixture was filtered off with filter paper, then the product was concentrated under vacuum to obtain a pale yellow liquid (6r). The product was used without further purification. The obtained products are shown in Scheme S2.
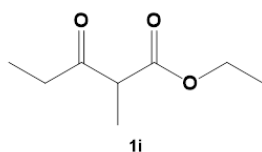
Scheme S2: Obtained products from methylation synthesis.

Finally, the synthetized compounds 1f, 1g, 1h and 1i were analysed by NMR (Figures S15-S18).

Determination of kinetic parameters

To determine the kinetic parameters of the enzymes, the redox activity was measured by monitoring the absorbance at 340 nm of NADH in the case of the TtHBDH and NADPH for LkKRED. The general enzymatic assay involved the reduction of a solution containing different concentrations (0.1-500 mM) of the tested substrates, 0.2 mM of either NADH or NADPH and 25 mM of sodium phosphate buffer at pH 7. Reactions were monitored by measuring absorbance at 340 nm, after adding 5 µL of soluble enzyme to 200 µL of the reaction solution in a 96-well plate. Each substrate concentration was assayed in triplicate, and the mean value for each substrate concentration was calculated. All mean activities were plotted and adjusted to a Michaelis-Menten or Michaelis-Menten with inhibition models using Origin Pro software.

Functionalization of agarose beads

Agarose macroporous microbeads (AG) 6BCL (50-150 µm diameter, 200 nm pore size) were functionalized following different strategies to immobilize both enzymes:

36

The activation was prepared as previously described using agarose 6BCL. Briefly, agarose was first activated with glyceryl groups by incubation at alkaline pH with glycidol. Then the obtained glyceryl groups were oxidized with 20 mM $NaIO_4$ (1 hour of incubation). An approximate group density of 100 µmol of glyoxyl groups per gram of agarose was obtained. [5]

Epoxy - Iminodiacetic acid – Cobalt chelates activated supports (AG-Co^{2+}/E).

6 BCL AG microbeads were initially activated with epoxy groups by incubation with an aqueous solution of 2 M Epichlorohydrin, 1 M NaOH, 0.088 M $NaBH_4$ and 3.6 M Acetone for 16h. The obtaine agarose epoxy (AG-E) was then incubated with 0.5M iminiodiacetic acid (IDA) at pH 11 for 30 min at room temperature and orbital shaking to produce agarose activated with epoxy and IDA groups (AG-E/IDA). Finally the beads were incubated with an aqueous solution of $CoCl_2$ (30 mg mL^{-1}) in a 1:10 (*w:v*) ratio with orbital shaking, to produce AG-Co$^{2+/}$E.

Construction of ssHB: Enzyme and cofactor immobilization protocols

The process of constructing a ssHB involves multiple stages, including enzyme immobilization, post-immobilization polymer coating, and cofactor immobilization.

ssHB of TtHBDH:

Immobilization on glyoxyl agarose (AG-G)

The immobilization was carried out by mixing a solution of 100 mM sodium bicarbonate pH 10 containing around 25 mg mL^{-1} of purified soluble TtHBDH with AG-G beads in a 1.10 (w*/v) ratio.* The suspension was gently stirred at 25 °C for 3 h and subsequently filtered. The concentration of immobilized enzyme was determined by subtracting the concentration of the supernatant from the offered enzyme concentration (measured through Bradford protein assay).

37

Post-immobilization coating

After the immobilization, TtHBDH@AG-G was incubated with a solution of 10 mg mL^{-1} of branched polyethyleneimine (PEI) (25 kDa) in 100 mM sodium bicarbonate pH 10 and incubated at 25 °C for 1 h under gentle stirring. Then, 1 mg mL^{-1} of solid NaBH$_4$ was added and incubated for 30 min at 4 °C to covalently immobilize the PEI and the enzyme on the support to yield (PEI)TtHBDH@AG-G. the completely reduced biocatalyst was vacuum filtered and washed with an excess of 10 mM Tris-HCl buffer at pH 7.

Cofactor immobilization

The previously prepared (PEI)TtHBDH@AG-G was incubated with a freshly prepared solution of 1 mM NADH in 10 mM Tris-HCl pH 7 for 1 h at 4 °C. Finally, the heterogeneous biocatalyst with the immobilised cofactor (TtHBDH@ssHB) was washed with 2 volumes of 10 mM Tris-HCl pH 7 buffer. The supernatants of the cofactor immobilization and the washing steps were analysed by UV-vis to quantify the amount of cofactor that was immobilized and then released during the washing steps.

ssHB of LkKRED:

Immobilization on AG-Co$^{2+/}$E:

LkKRED was immobilized directly from the soluble crude protein extract in complex buffer (100 mM Tris-HCl buffer, 200mM NaCl, 1 mM MgCl$_2$) at pH 7. The protein solution was incubated with AG-Co$^{2+/}$E in a ratio of 1:10 (*w/v*) for 1 h at 4°C, then the suspension was filtered and the supernatant collected for further analysis. Then the heterogeneous biocatalyst was washed with the same buffer. The concentration of immobilized enzyme was determined by subtracting the concentration of the supernatant from the offered enzyme concentration (measured through Bradford protein assay).

Post-immobilization coating:

The immobilized enzyme (LkKRED@AG-Co^{2+}/E) was incubated with a solution of polyallylamine 65 kDa (PAH) of 10 mg mL^{-1} at pH 8 in a 1:10 (*w/v*) ratio for 1 h at room temperature as previously described. [6]

Cofactor immobilization

The previously prepared (PAH)LkKRED@AG-Co^{2+}/E was incubated with a freshly prepared solution of 1 mM NADH in 10 mM Tris-HCl pH 7 for 1 h at 4 °C. Finally, the heterogeneous biocatalyst with the immobilised cofactor (LkKRED@ssHB) was washed with 2 volumes of 10 mM Tris-HCl pH 7 buffer. The supernatants of the immobilization and the washing step were analysed by UV-Vis to quantify the amount of cofactor that was immobilized and released during the washing steps.

Calculation of immobilization parameters

The immobilization parameters characterized in this study (Table 2) were calculated as follows:[7]

- **Load** is the mass (mg) of enzyme immobilized per gram of support.

$$Load \ (mg \ g^{-1}) = \left(offered \ enzyme \ (mg \ mL^{-1}) - \ enzyme \ in \ supernatant \ (mg \ mL^{-1})\right) x \ \frac{immobilization \ volume \ (mL)}{mass \ of \ support \ (g^{-1})} \quad [1]$$

- **Immobilization yield (Ψ)** is the percentage of the offered enzyme that is immobilized on the support. The concentration of enzyme offered or remaining in the supernatant after immobilisation was calculated by the Bradford protein assay.

$$\Psi = 100 \ x \frac{offered \ enzyme \ (mg \ mL^{-1}) - enzyme \ in \ supernatant \ (mg \ mL^{-1})}{offered \ enzyme \ (mg \ mL^{-1})} \quad [2]$$

- **Recovered activity (Ar)** is defined as the measured enzyme activity per gram of carrier and is expressed in U g^{-1} . The determination of the immobilized enzyme activity was done as described in enzyme activity assay section but with minor modifications: 10µL of a 1.10 (*w/v*) suspension of the heterogeneous biocatalyst were place in the well instead of the 5 µL of soluble enzyme.

39

- **Immobilized specific activity (iSA)** is defined as the activity per mg of immobilized enzyme.

$$iSA\ (U\ mg^{-1}) = A_r\ (U\ g^{-1})\ x\ Load\ (mg\ g^{-1}) \qquad [3]$$

- **Relative specific activity (%)** is defined as the ratio between iSA and the free enzyme specific activity

$$rSA\ \% = \frac{iSA}{soluble\ enzyme\ SA}\ x\ 100 \qquad [4]$$

- **Immobilized cofactor:** Amount of cofactor (µmol) immobilized per gram of support.

$$A_{340} = c_{NAD(P)H} \cdot l \cdot \varepsilon_{NADH} \ \rightarrow \ \mu mol_{\ NAD(P)H} = \frac{A \cdot Vol}{l \cdot \varepsilon} \qquad [5]$$

$$Immobilized\ cofactor\ \left(\frac{\mu mol\ NAD(P)H}{g\ Het.Biocatalyst}\right) = \frac{\mu mol\ NADH_{\ offered} - \mu mol\ NADH_{\ flowtrought} - \mu mol\ NADH_{\ washed}}{g\ Heterogeneous\ Biocatalyst} \qquad [6]$$

LkKRED@ssHB Batch Reaction course

To obtain the reaction course of the asymmetric reduction of 1a by LkKRED@ssHB, 100 mg of solid LkKRED self-sufficient heterogeneous biocatalyst were placed in a micro chromatographic column (Biospin TM, BIO-RAD). The reaction was triggered by adding 1 mL of reaction mixture composed of 200 mM of ethyl acetoacetate (1a) , 5% (v/v) of isopropyl alcohol in a 10 mM Tris-HCl buffer at pH 7.0. Several samples were withdrawn at different times from the reaction bulk by vacuum filtration but never removing more than 5% of the total reaction volume. The samples were analysed by GC-FID as described in the following section.

GC-FID analysis
We analysed the reaction samples using gas chromatograph with a flame ionization detector (GC-FID). Each sample was extracted (liquid-liquid) with dichloromethane in a 1:1 (*v:v*) ratio, the aqueous phase was discarded. 50 mg of anhydrous $MgSO_4$ were added to the organic phase to dry the samples. Analyses were carried out in an Agilent

40

8890 gas chromatography system as described previously.[1] Briefly, we used a column

of (5%-phenyl)-methylpolysiloxane (Agilent, J&W HP-5 30 m × 0.32 mm × 25 μm),

helium as the carrier gas (1.5 mL min^{-1}) and equipped with an FID detector. The

temperatures of the injector and FID detector were 280 °C and 300 °C, respectively.

The separation of compounds was carried out by two sequential temperature ramps: the

initial temperature (60 °C) was maintained for 2 min and progressively increased up to

160 °C at a rate of 10 °C min$^{-1.}$ Then, the column temperature was increased to 20 °C

min^{-1} for 4 min until 250 °C and maintained for 4 min. Retention times were 3.4 min

for ethyl acetoacetate (1a) and 3.29 min for ethyl 3-hydroxybutyrate (2a).

Chromatographic Yield and Space-Time Yield calculation
Some parameters such as Chromatographic Yield (CY) (%), space-time yield (STY),
were calculated according to the following equations:

$$CY\ (\%)\ =\ \frac{\mu mol\ product}{\mu mol\ product\ +\ \mu mol\ substrate}\ x\ 100 \qquad [7]$$

$$STY\ (g\ L\ h^{-1}) = \frac{Product\ concentration\ (g/L)}{\tau\ (h)} \qquad [8]$$

Chiral GC-analysis
The enantioselectivity of LkKRED@ssHB in the reduction of 1a was determined by

GC-FID. 500 μL of the reaction sample or a solution of enantiopure commercial

standards (100mM (*R*) or (*S*) ethyl 3-hydroxybutyrate) were incubated with 500 μL of

ethyl acetate for liquid-liquid extraction. 200μL of the extracted sample were analysed

by GC-FID as previously described{Orrego, 2023 #100} in an Agilent 8890 System

using a Beta DEXTM 120 Capillary Column (30 m x 0.25 mm x 0.25 μm) and helium

as carrier gas. The temperature of the injector and FID detector was 280°C and 300°C

respectively. the initial temperature (80 °C) was progressively increased up to 150 °C at

a rate of 2 °C min^{-1} , then it was maintained for 5 minutes before increasing the

temperature up to 200 ℃ at a 20 °C min^{-1} rate, the oven temperature was maintained at

41

200 ºC for 2 minutes. The retention times were 10.85 (ethyl (*S*)-3-hydroxy butyrate) and 10.95 for (ethyl (*R*)-3-hydroxy butyrate).

Kinetic parameters of ssHB

To determine the Michaelis-Menten parameters in the reduction of 1a, 50 mg of solid either TtHBDH or LkKRED self-sufficient heterogeneous biocatalysts ($\sim$ 25 $mg_{protein} \times g_{carrier}^{-1}$) were placed in a micro chromatographic column (Biospin TM, BIO-RAD). The reaction was triggered by adding 500 µL of reaction mixture composed of different concentrations (1-1000 mM) of 1a, 5% (*v/v*) of isopropyl alcohol in a 10 mM Tris-HCl buffer at pH 7. For TtHBDH@ssHB reactions were incubated for 0.5 h at 50 °C under gently orbital agitation. To obtain always less than 30 % conversion, in the case of LkKRED@ssHB, reaction times were modified depending of substrate concentration: 2 min for reactions with low substrate concentrations (1, 5 mM); 5 min for medium substrate concentrations (10, 20, 50 mM) or 10 min for reactions with high substrate concentration (100, 250, 500, 1000mM) . The reactions were then stopped by vacuum filtration and analysed by GC-FID as described above.

Set-up of continuous flow reactions

For analyzing the performance of ssHBs in continuous flow process, we built two packed bed reactors (PBR) by packing 1 g of solid TtHBDH ssHB or 0.5g of LkKRED ssHB in 9 mm diameter columns with a final reactor volume (Vr) of 1.4 mL or 0.7 mL respectively. In the case of TtHBDH PBR, three reaction mixtures containing different amount of 1a (50, 200 or 1000 mM); Isopropanol (5, 5 or 10 % (*v/v*) respectively*)* but always in 10 mM Tris-HCl pH 7 buffer were pumped through the PBR with a syringe pump 11-PLUS, Harvard apparatus (Massachusetts) at different flow rates (0.01, 0.05, 0.1, 0.2 mL min^{-1}). Each column was flushed with 2 colum volumes for each flow rate to assure the perfect equilibration of the PBR. The eluted volume was passed through an

42

on-line spectrophotometer (360 nm) (Essi tech, Slovenia), collected in different aliquots, and analysed by GC-FID as previously described. The same procedure was applied to the LkKRED@ssHB PBR reactor at a fixed substrate (1a) concentration of 200 mM (5% (*v/v*) isopropanol in 10mM Tris-HCl pH 7) , maintaining the flow rate variations.

The residence times (τ) of the different conditions were analysed with the following equation:

$$\tau \ (min) = \frac{Reactor\ volume\ (mL)}{Flow\ rate\ (mL\ min^{-1})} \qquad [9]$$

Simulation of reaction kinetics of SSHBs.

The conversion of substrate 1a (A) catalyzed by TtHBDH@ssHB and LkKRED@ssHB was simulated by using a kinetic model coupled to reactor mass balance. The reaction kinetic equations and kinetic models used are shown in the following table:

Model	Reactor kinetic equation	Kinetic model
S + P inhibition (Batch reactor and ideal plug flow reactor)	$\tau = C_{A0} \int_0^{x_A} \frac{dX_A}{r}$ [10]	$r = \dfrac{V_{max}}{C_A(1+\frac{C_A}{K_S})+K_m(1+\frac{C_{A0}-C_A}{K_p})}$ [11]
S + P inhibition + full axial dispersion Flow reactor with full axial dispersion)	$\tau = \dfrac{C_{A0}}{r} X_A$ [12]	$r = \dfrac{V_{max}}{C_A(1+\frac{C_A}{K_S})+K_m(1+\frac{C_{A0}-C_A}{K_p})}$ [13]

The results were expressed in terms of conversion versus dimensionless reaction time, Da_I, which is the first Damköhler number given by the ratio between the reaction residence time (τ) and the characteristic reactor time ($\tau_{characteristic}$).

The characteristic reaction time ($\tau_{characteristic}$) is given by the ratio of substrate concentration to v_{max} and indicates the minimum time to reach 100% conversion if the enzyme kinetics would respond to a zero reaction order.

$$Da_I = \frac{\tau}{\tau_{characteristic}} = \frac{\tau\ V_{max}}{C_{A0}} \qquad [14]$$

The kinetic constant values are described in Table S4.

43

For the numerical integration of the reactor kinetic equation was carried out by using the software Berkely Madonna (Version 10.4.2) by using a 4th order Runge-Kutta algorithm. A single response fitting was performed by using the tool "curve fit" for the calculation of the product inhibition kinetic constant.

Product inhibition determination

50 mg of solid either TtHBDH or LkKRED self-sufficient heterogeneous biocatalysts (~25 $mg_{protein} \times g_{carrier}^{-1}$) were placed in a micro chromatographic column (Biospin TM, BIO-RAD). The reaction was triggered by adding 500 µL of reaction mixture composed of different concentrations (1-500mM) of ethyl 3-hydroxybutyrate (2a), 200 mM of ethyl acetoacetate (1a), 5% (*v/v*) of isopropanol in a 10 mM Tris-HCl buffer at pH 7.0. To always obtain conversions below 30 %，TtHBDH@ssHB reactions were incubated for 0.5 h at 50 °C under gently orbital agitation and LkKRED@ssHB reactions were incubated for 10 min at 25 ℃. The reactions were then stopped by vacuum filtration and analysed by GC-FID.

Operational stability of Continuous flow reactions set-up

For analyzing the performance of ssHBs in long operations, we prepared packed bed reactors as described above with 1g of either TtHBDH@ssHB or LkKRED@ssHB (Vr = 1.4 mL). The reaction mixture (200 mM 1a, 5% (*v/v*) Isopropanol; 10 mM Tris-HCl buffer pH 7) was pumped through the reactor with a peristaltic pump, previously calibrated, at a maintained flow rate of 0.05 mL min⁻¹ with an average retention time (τ) of 28 minutes. The collected aliquots were analysed by GC-FID as described above and the following parameters were calculated:

$$Specific\ Productivity\ (SP) = \frac{STY}{[enzyme]} \qquad [15]$$

$$TTN_{Enzyme} = \frac{mol\ Product}{mol\ Enzyme} \qquad [16]$$

$$TTN_{NAD(P)H} = \frac{mol\ Product}{mol\ NAD(P)H} \qquad [17]$$

44

In the operation of TtHBDH@ssHB, the reaction crude obtained was purified with three extractions with diethyl ether 1:1 (*v/v*). The organic phases were gathered and dried over anhydrous Na_2SO_4. The solvent was removed in vacuo, and the crude was purified by column chromatography (Hexane/Ethyl acetate: from 90:10 to 80:20).

Post-operation ssHB analysis

After the long-operation, the used TtHBDH@ssHB was carefully extracted from the reactor to enable segregation into the inlet, intermediate, and outlet sections. These samples were subjected to two procedures: firstly, the evaluation of the remaining enzyme activity as previously outlined, and secondly, the lixiviation of the remaining cofactor by incubating 1.10 (*w/v*) with 1M NaCl. Following the lixiviation of the cofactor, all the samples of the heterogeneous biocatalyst were incubated with 1 mM NADH as previously described, to re-immobilize fresh NADH and test the activity in continuous flow operation under identical conditions as described earlier.

UPLC-Ms analysis of eluted NADH

The solution with the lixiviated cofactor was analyzed by UPLC-MS. Ultra-performance liquid chromatography coupled to mass spectrometry (UPLC-MS). using an Acquity UPLC equipped with a photodiode array detector (PDA) and a time-of-flight mass spectrometer (ESI-TOF) LCT Premier XE from Waters. The gradients elution buffers were (A) 100 mM ammonium formate and (B) acetonitrile. The following gradient program was used at a 0.3 mL min^{-1} : from 0 to 1 min, isocratic at 95 % A; from 1 to 14 min, gradient to 80 % A; from 14 to 15 min, gradient to 10 % A; from 15 to 17 min, isocratic at 10 % A; from 17 to 17.5 min, gradient back to 95% A; from 17.5 to 20 min, stabilization at 95% A. 5 µL of samples were injected and NADH and its degradation fragments were detected at 340 nm and its molecular mass were confirmed

45

by ESI-TOF MS. Mass spectrometry detection was performed using a time-of-flight mass spectrometer (ESI-TOF) LCT Premier XE with an electrospray ionization source, working in positive mode. The MS range was between m/z 100 and 1000 Da. The capillary and cone voltages were set at 3000 and 100 V, respectively. The desolvation gas temperature was 220 °C, and the source temperature was 120 °C. The desolvation gas flow was set at 600 L h^{-1} , and the cone gas flow was set at 50 L h^{-1}. Quantification and data analysis were done in Masslynx version 4.1.

In-operando under microscope setup

We build a reactor by modifying one of the ends of a channel μ-slides Luer I$^{0.4}$ (Ibidi, Gräfelfing, Germany) with dimensions: length 50 mm; width 5 mm. height: 0.4 mm with a 0.45 µm filter to prevent beads lixiviation. Then, we pumped a 1.20 (w/v) suspension of TtHBDH@ssHB in 10 mM Tris-HCl buffer pH 7 through the channel until we completely filled it with biocatalyst, obtaining a packed bed reactor (Vr = 0.1 mL). The reaction mixture (200mM 1a, 5% (*v/v*) Isopropanol ; 10 mM Tris-HCl buffer pH 7) was pumped through the reactor with a syringe pump 11-PLUS, Harvard apparatus (Massachusetts), previously calibrated, at a maintained flow rate of 0.003 mL min^{-1} with an average retention time (τ) of 30 minutes. The reactors were operated at 30 ºC or 50 ºC for 24 h and then analysed with epifluorescence microscopy. The autofluorescence of NADH was followed using epifluorescence microscopy with a ZEISS Axio Observer microscope(Carl Zeiss, Germany) and a excitation Colibri 5 led system of $\lambda_{ex} = 385$ nm.

Green Metrics calculation and formula

The sustainability of the synthesis of ethyl 3-hdyroxybutyrate in the long-term

continuous flow operations with TtHBDH@ssHB and LkKRED@ssHB was determined

by calculating the E factor with the following parameters and equations:

- Product mass: Amount of product obtained after the whole continuous process
  operation.

- Waste mass: the total sum of the mass of reagents, water and catalyst involved in
  the process minus the product mass.

$$E\ factor = \frac{Waste\ mass}{Product\ mass} \qquad [18]$$

The dissected E factor was obtained by division of the mass of each contributor by the

mass of the products according to the following equations:

$$E\ factor\ reagents = \frac{Reagents\ mass}{Product\ mass} \qquad [19]$$

$$E\ factor\ water = \frac{Water\ mass}{Product\ mass} \qquad [20]$$

$$E\ factor\ catalyst = \frac{Catalyst\ mass}{Product\ mass} \qquad [21]$$

Supporting Tables

Table S1: Enzyme sequences

Enzyme	Sequence
(S)-3-hydroxybutyryl-CoA dehydrogenase from *Thermus thermophilus* HB27 **(TtHBDH)**	MGEVKRIGVVGAGQMGSGIAQVAASAGYEVVLVDVAESFLERGLAAIRRSLGKFLEKGKITQEAHDEALGRIR TSLSLEDLKDADLIVEAIVEDEGEKRRLFERLGALAKPEAILASNTSSIPITALARYSGRPERFIGMHFFNPVPLM QLVEVIRGELTSEATRDVVVEVARRMGKTPLEVQDYPGFISNRLLMPMINEAIEALREGVATKEAIDGIMRLGM NHPMGPLELADFIGLDTCLAIMEVLHRGFGDDKYRPSPLLRRMVQAGLLGRKAGRGFYTYDEKGNKVGL

| Ketoreductase from *Lactobacillus kefir* (**LkKRED**) | MGSSHHHHHHSSGLVPRGSHMTGFTAANTTYTLNNGVRIPAVGFGTFANEGAKGETYAAVKKALEVGYRHL DCAWFYQNEDEVGQALAEFLENHKDVKREDIFICTKVVWNHLHEPEDVKWSLQNSLDKLKVDYVDLFLIHWPI AAEKDEATNMPKIGPDGKYIIKKELTENPEPTWRAMEDLVDAGKTRSIGVSNWTIPGLQKLLKFARIKPTVNQI EIHPFLPNTELVEFCFKNQIIPTAYSPLGSQNQVPSTGERVRDDPTLKAVAERSGHNLAQVLLAWGLRRGYVV LPKSSTPSRIESNFQIPVLRDEDFKAIQEVAKGRHCRFVNMKDTFGYDVWPEESDGQLKQE |

Table S2: Kinetic parameters of simulations

		TtHBDH	LkKRED
K_M	mM	65,6	7,03
CAo	mM	200	200
K_S	mM	584	418,6
V_{max} reactor batch	mM h^{-1}	117,9	118
V_{max} reactor Flow dispersion	mM h^{-1}	926,4	927
K_P	mM	117	30

Table S3: Comparative metrics of different ssHBs in asymmetric reductions in continuous flow found in the literature.

		COFACTOR	Media	STY (g L^{-1} h^{-1})	TTN$_{enzyme}$ (mol mol^{-1})	TTN$_{cofactor}$ (mol mol^{-1})
a	https://doi.org/10.1002/ange.202211912	NADP+	Buffer / Org. Solv.	5,54*	Nd	59204
b	https://doi.org/10.1002/cssc.202201654	NADP+	Buffer	46,3*	Nd	4800
c	https://doi.org/10.1002/cctc.201500766	NADH	Buffer	1*	90000	655
d	https://doi.org/10.1002/anie.201810331	NAD	Buffer	5*	nd	14000
e	https://doi.org/10.1021/acsnano.5b01278	NADH	Buffer	nd	Nd	9,4
f	https://doi.org/10.1002/anie.201609758	NAD+	Buffer	1,8	30000*	85
g	https://doi.org/10.1002/adsc.202000058	NADPH	Buffer/ Org. Solv.	121	nd	12855
h	https://doi.org/10.1038/s41929-019-0353-0	NAD+	Buffer	10,75*	1700*	10839
TtHBDH	this work	NADH	Buffer	37,5**	146000	2984
LkKRED	this work	NADP+	Buffer	37.4**	937354	27240
* Calculated from available data in publication. ** Average during operation time						

Table S4: Metrics of the continuous synthesis of (*R*) and (*S*) enantiomers of Ethyl 3-hydroxybutyrate

|	TtHBDH	LkKRED	Reference
Titre* (mass product/reaction volume) (Average)	19,5 g L^{-1}	24,7 g L^{-1}	10–50 g L^{-1}
Rate** (mass product/reaction volume/reaction time)	49 - 27 g L^{-1} h^{-1}	49.5 – 25.3 g L^{-1} h^{-1}	1–10 g L^{-1} h^{-1}
Yield (mass product/mass substrate) (Average)	95 - 49 %	90.2 - 46 %	> 90%
Specific yield*** (mass product/mass enzyme)	>101,5 g $g_{protein}^{-1}$	1169 g $g_{protein}^{-1}$	50 – 500 g $g_{protein}^{-1}$
TTN enzyme (mol mol^{-1})	146532	937354	10000
TTN NADH (mol mol^{-1})	2984	27240	1000
E factor	52,5	57.8	30

Supporting Figures
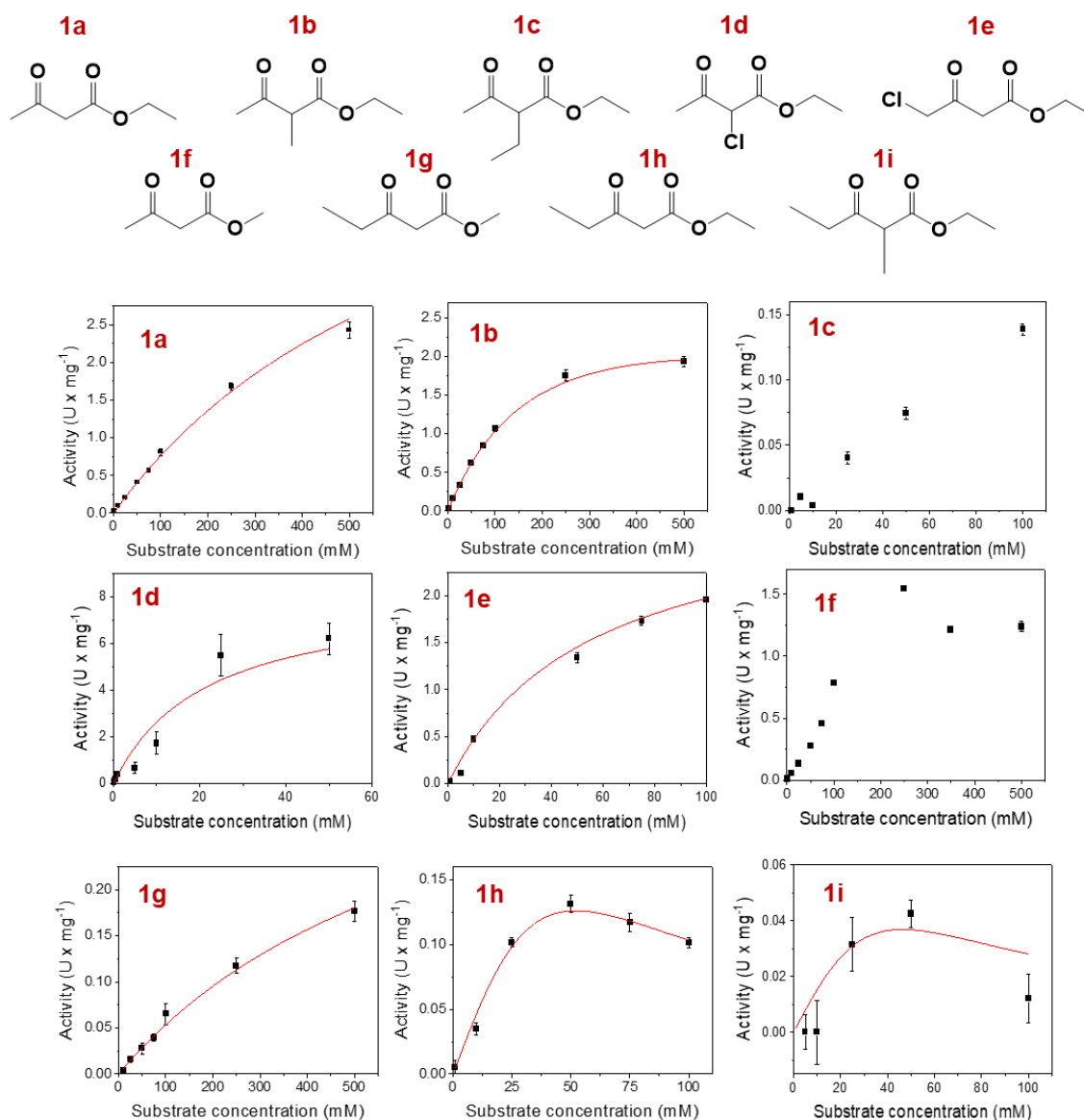
Figure S1. Michaelis-Menten curves of TtHBDH for different β-keto esters.

Reductive steady-state kinetics were calculated towards different concentrations of substrates (0.1-500 mM), with 0.2 mM of NADH in 25 mM sodium phosphate buffer at pH 7. The activities for each substrate concentration were done by triplicate at 30 ºC, resulting in a mean value for each substrate concentration. All mean activities were

plotted and adjusted to a Michaelis-Menten or Michaelis-Menten with inhibition models using Origin Pro software.
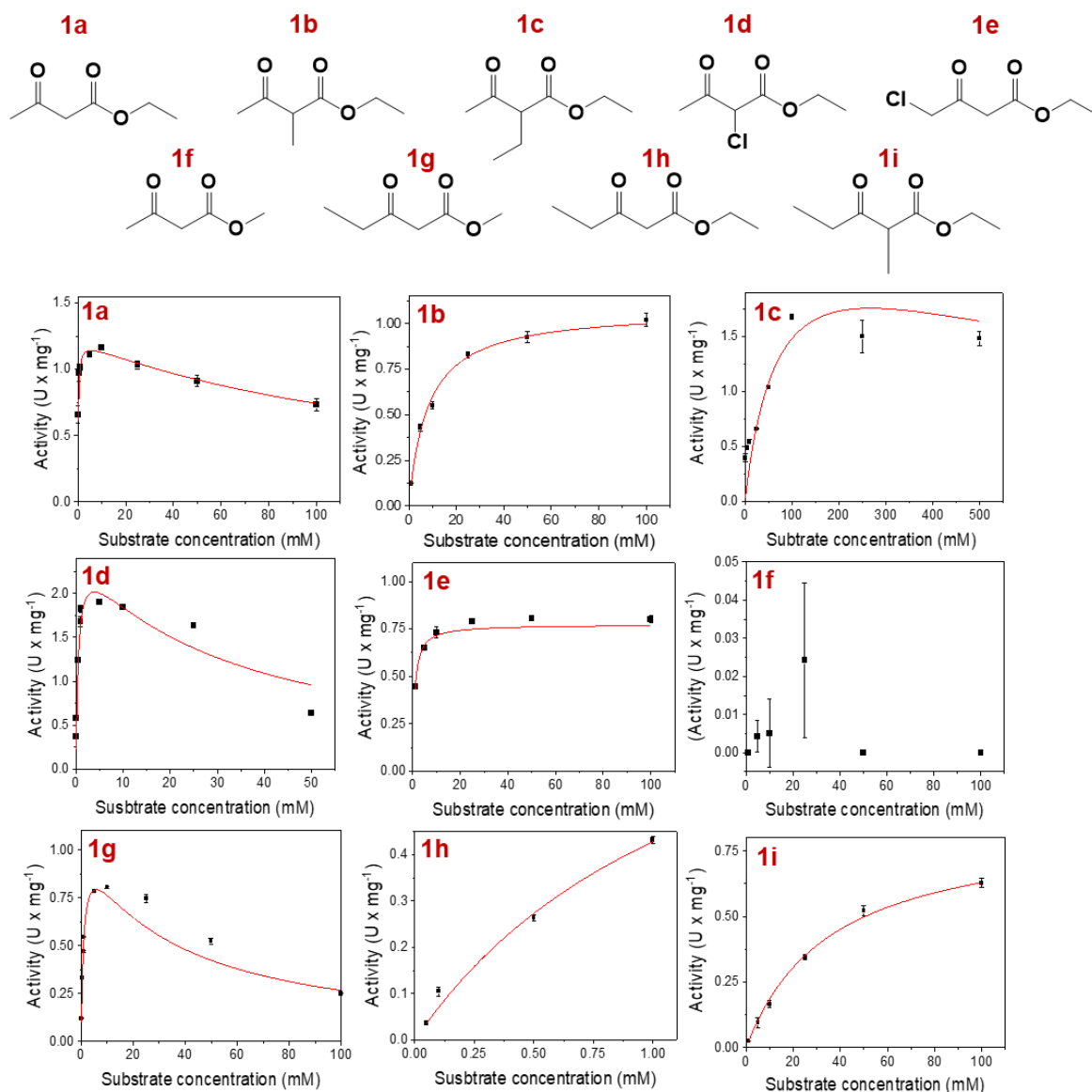
Figure S2. Michaelis-Menten curves of LkKRED for different β-keto esters.

Reductive steady-state kinetics were calculated towards different concentrations of substrates (0.1-500 mM), with 0,2 mM of NADPH in 25 mM sodium phosphate buffer at pH 7. The activities for each substrate concentration were done by triplicate at 30 ºC, resulting in a mean value for each substrate concentration. All mean activities were plotted and adjusted to a Michaelis-Menten or Michaelis-Menten with inhibition models using Origin Pro software.

50
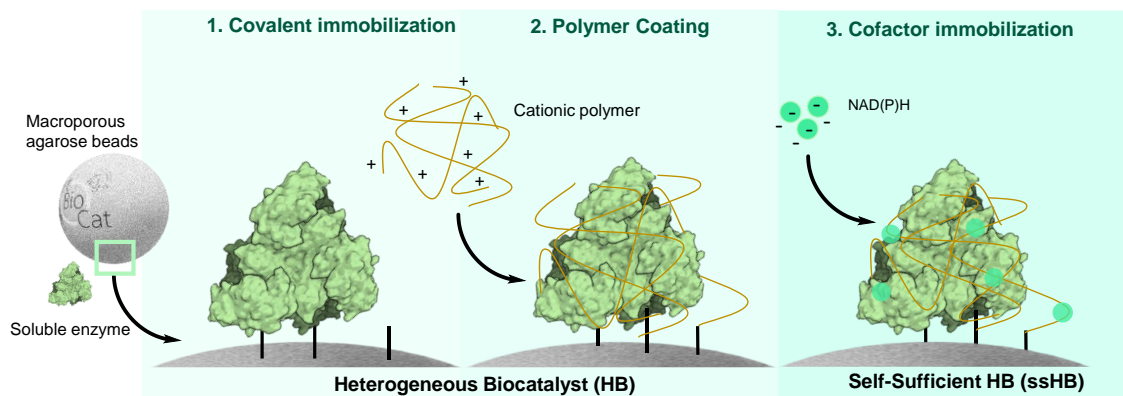
Figure S3. Construction steps of a Self-Sufficient Heterogeneous Biocatalyst.
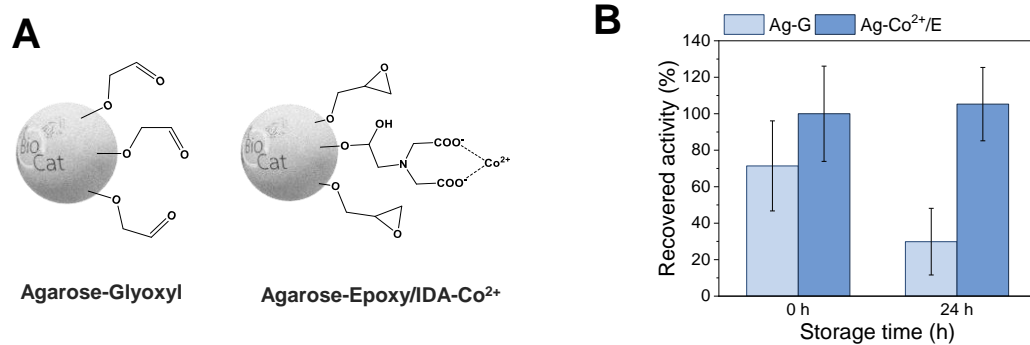
Figure S4. Agarose functionalization and stability of immobilised LkKRED.

(A) Functionalization of the agarose-porous beads employed on the construction of the ssHB with glyoxyl groups or with epoxy groups and cobalt chelates. (B) Recovered activity of immobilised LkKRED after 24 h storage at 4 ºC. The activity was measured with spectrophotometric assay as described in methods.

52
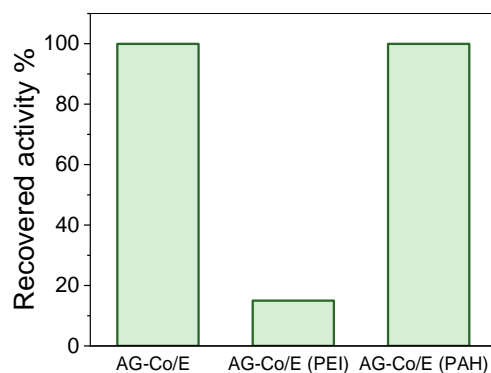
Figure S5. Recovered activity of immobilized LkKRED after post-immobilization coating.

The enzymatic activity of LkKRED immobilized and coated with different cationic polymers was analysed in the reduction of 1a. The activity was measured with spectrophotometric assays as described in Materials and Methods.

53
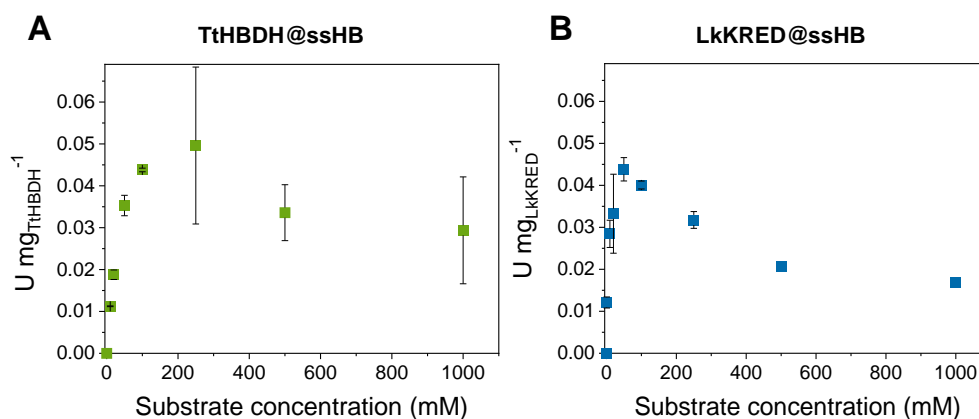
Figure S6. Michaelis-Menten curves of TtHBDH (A) and LkKRED (B) ssHBs.

Reductive steady-state kinetics were calculated by incubating 100 mg of ssHBs with solutions with different concentrations of ethyl acetoacetate (1a) (1-1000 mM) in 10 mM Tris-HCl buffer at pH 7. The cofactors (NADH for TtHBDH and NADPH for LkRED) were immobilized at 6.5 and 8.1 μmol_{NADH} per gram of ssHB. The reactions were incubated for 30 min (TtHBDH) or 10 min (LkKRED) and made by duplicate. All mean activities were plotted and adjusted to a Michaelis-Menten or Michaelis-Menten with inhibition models using Origin Pro software (fitting not shown).

54
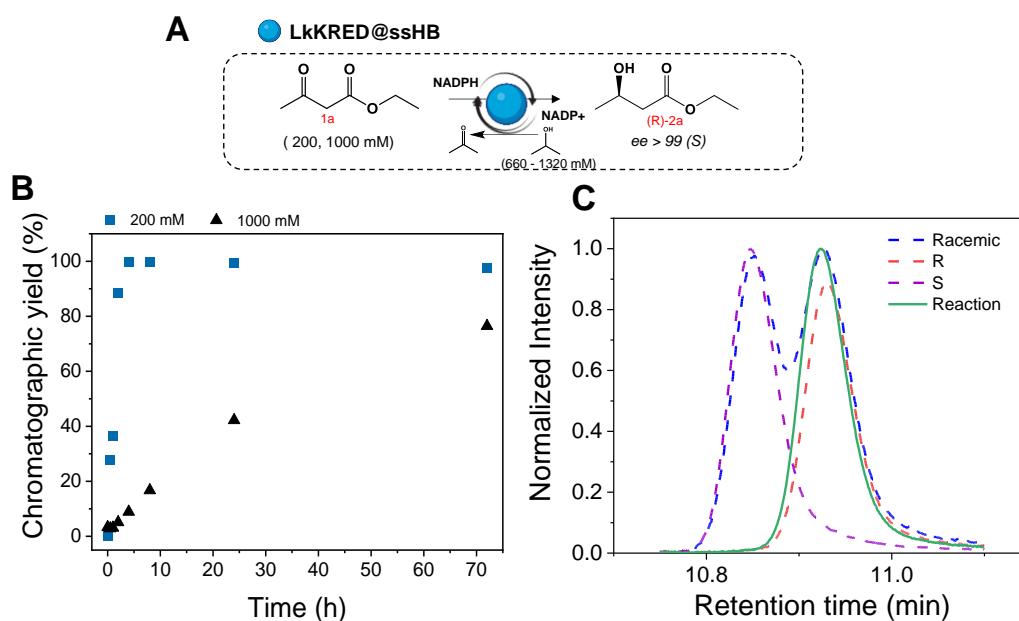
Figure S7. Reaction scheme, Reaction course and Chirality analysis of LkKRED@ssHB reduction of 1a.

(A) Reaction scheme of asymmetric reduction of 1a by LkKRED self-sufficient heterogeneous biocatalyst with cofactor recycling based in Isopropanol oxidation. (B) 100 mg of the ssHB described in Table 2 were incubated for 72 h with 1 mL of a solution of (200-1000 mM) ethyl acetoacetate (1a) in 10 mM Tris-HCl buffer at pH 7. Several aliquotes of less than a 5% of the total reaction volume were withdrawn and analysed by GC-FID as described in materials and methods. (C) The final product of the previous reactions in addition to racemic, (*S*)- and (*R*) ethyl 3-hydroxybutyrate (2a) standards were derivatized as described in materials and methods and analyzed by chiral GC-FID.
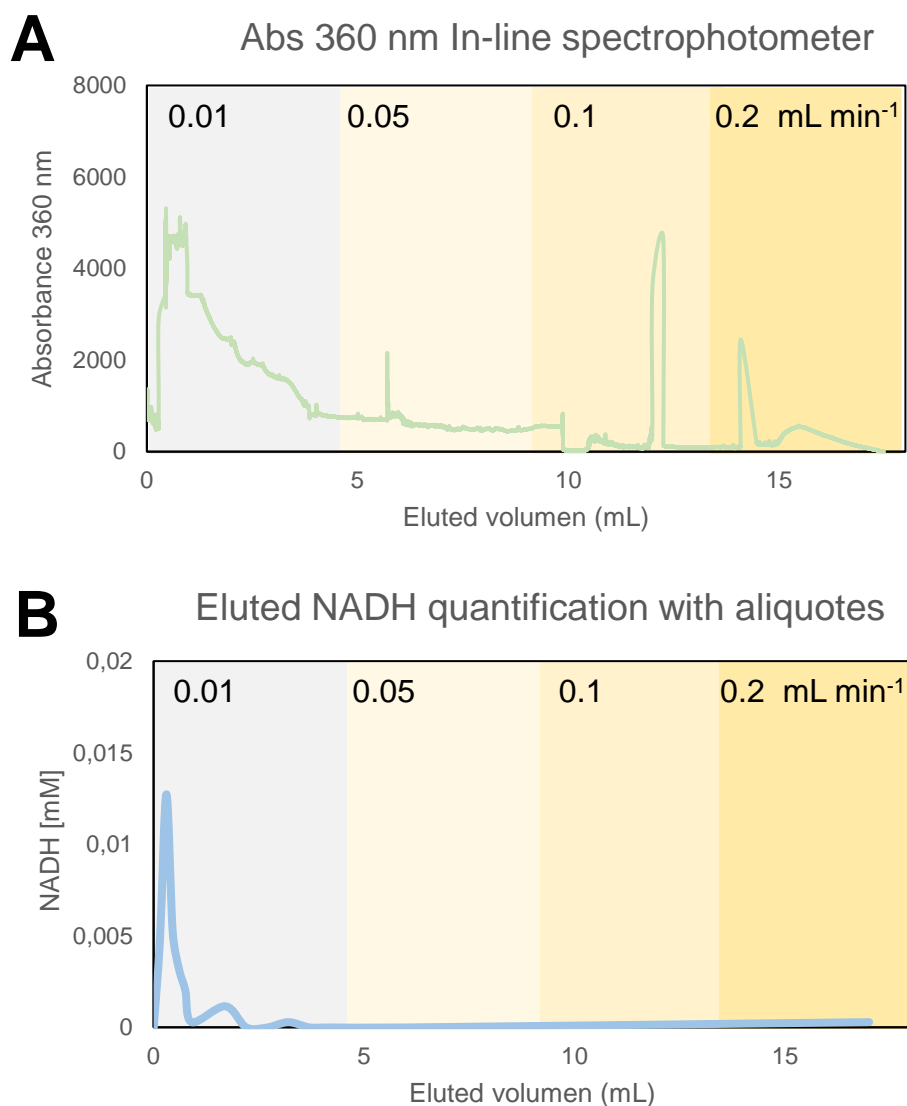
Figure S8. Eluted NADH during continuous flow optimization 200 mM 1a reduction at different flow rates with TtHBDH ssHB

A) Absorbance (360 nm) detected by In-line spectrophotometer during continuous flow experiments . B) Concentration of NADH eluted vs eluted volume measured by determination of Abs 340 nm in the collected aliquots.
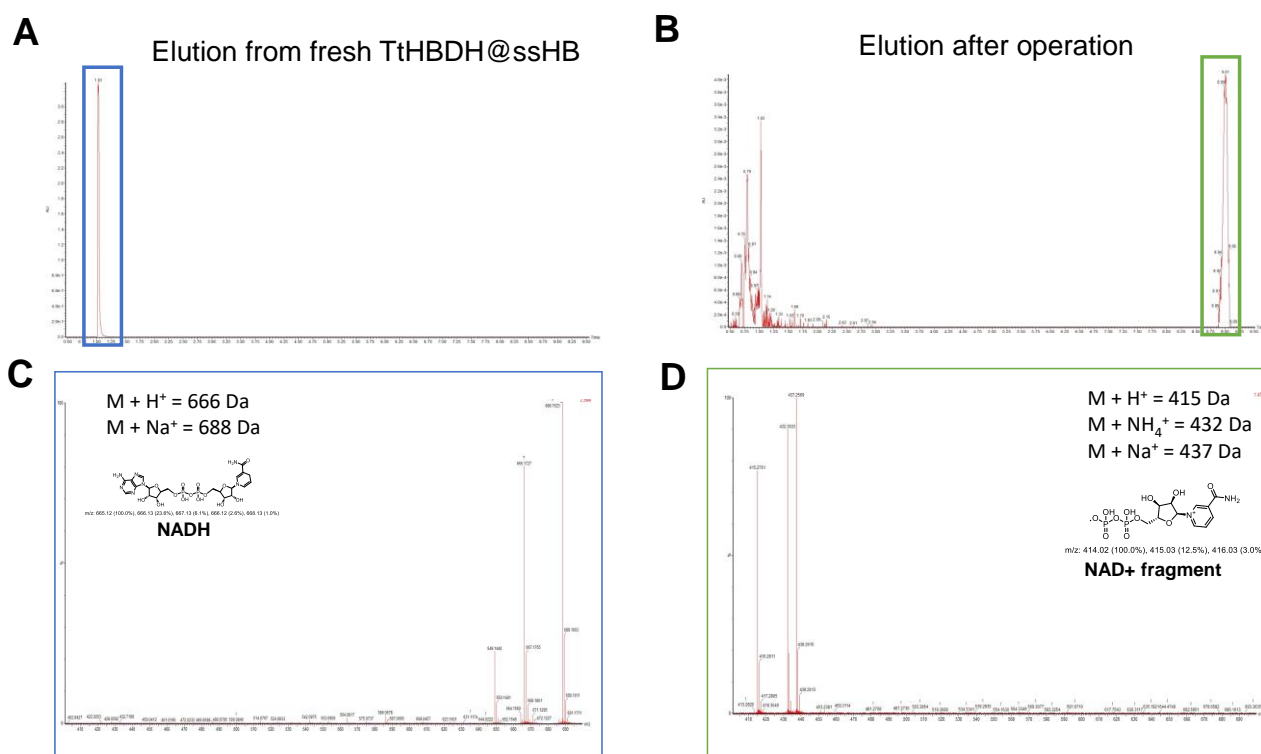
56
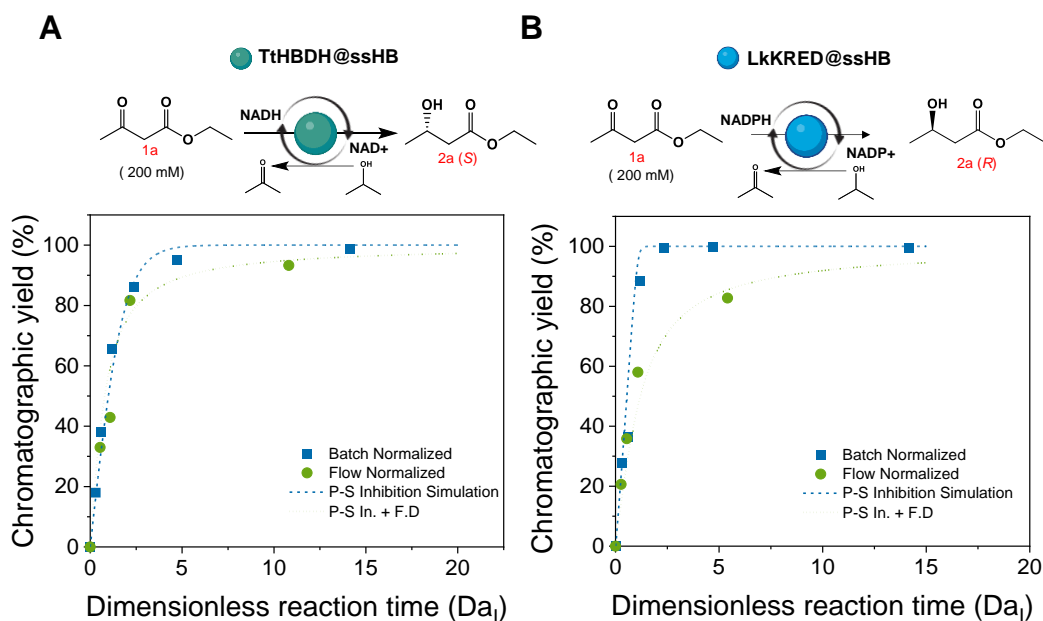
Figure S9. Comparison of simulated (dashed line) and real (square/circle) data of 1a conversion

To enable a proper comparison between batch and continuous flow reactions we plotted the conversion vs. dimensionless reaction time (first Damköhler number) calculated dependent on reactor type and residence time. We compared the real data of the TtHBDH (A) or LkKRED (B) ssHBs in batch reactions (circles) or packed bed reactor (squares) with the first order reaction simulated employing a kinetic model of Michaelis-Menten with substrate and product inhibition in the absence (blue dashed line) or presence (green dots line) of flow dispersion. These results were simulated using the kinetics constants obtained for the immobilized enzymes.
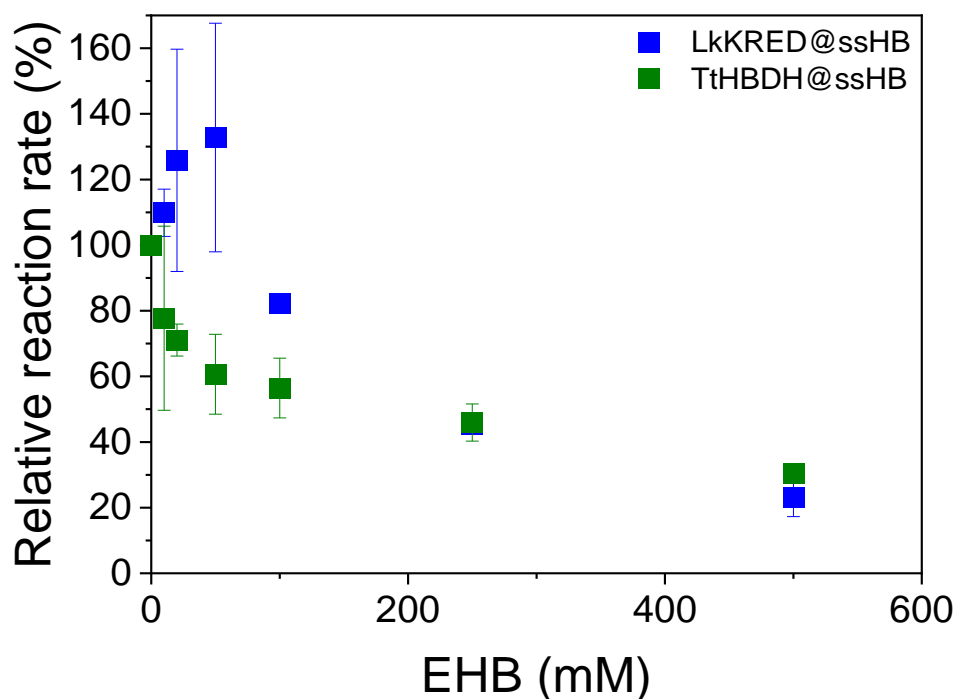
Figure S10. Relative reaction rate of TtHBDH (Green) and LkKRED (Blue) ssHB in the presence of different concentrations of 2a.

100 mg of the ssHB were incubated for 30 min with 1 mL of a solution of ethyl acetoacetate (1a) (200 mM) in 10 mM Tris-HCl buffer at pH 7, in the presence of different concentrations of 2a (10-500 mM). The reaction was stopped by filtration and analysed by GC-FID.

A Elution from fresh TtHBDH@ssHB

B Elution after operation

C

M + H⁺ = 666 Da
M + Na⁺ = 688 Da

m/z: 665.12 (100.0%), 666.13 (23.8%), 667.13 (8.1%), 666.12 (2.8%), 668.13 (1.0%)

NADH

D

M + H⁺ = 415 Da
M + NH₄⁺ = 432 Da
M + Na⁺ = 437 Da

m/z: 414.02 (100.0%), 415.03 (12.5%), 416.03 (3.0%)

NAD+ fragment

Figure S11. UPLC-Ms analysis of eluted NADH

UPLC-MS chromatograms at 340 nm of the supernatants recovered after incubation with 1M NaCl of fresh (A) and used (B) TtHBDH@ssHB. Positive ion TOF-MS spectra of peaks squared in blue from A (C) or in green from B (D).

59
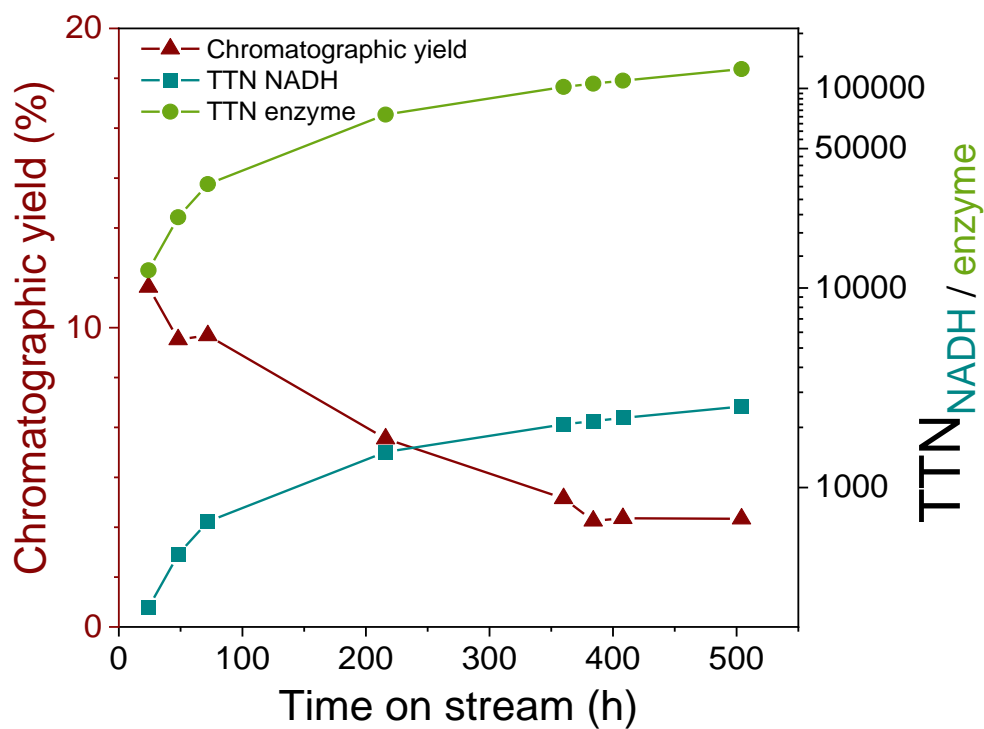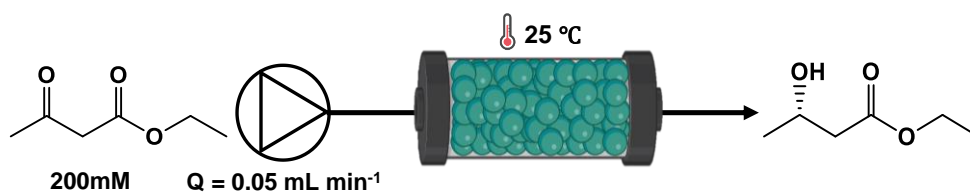
Figure S12. Continuous operation of TtHBDH@ssHB at 25ºC

Chromatographic Yield vs TTN of enzyme and cofactor of TtHBDH@ssHB in the reduction of 200mM of **1a**.
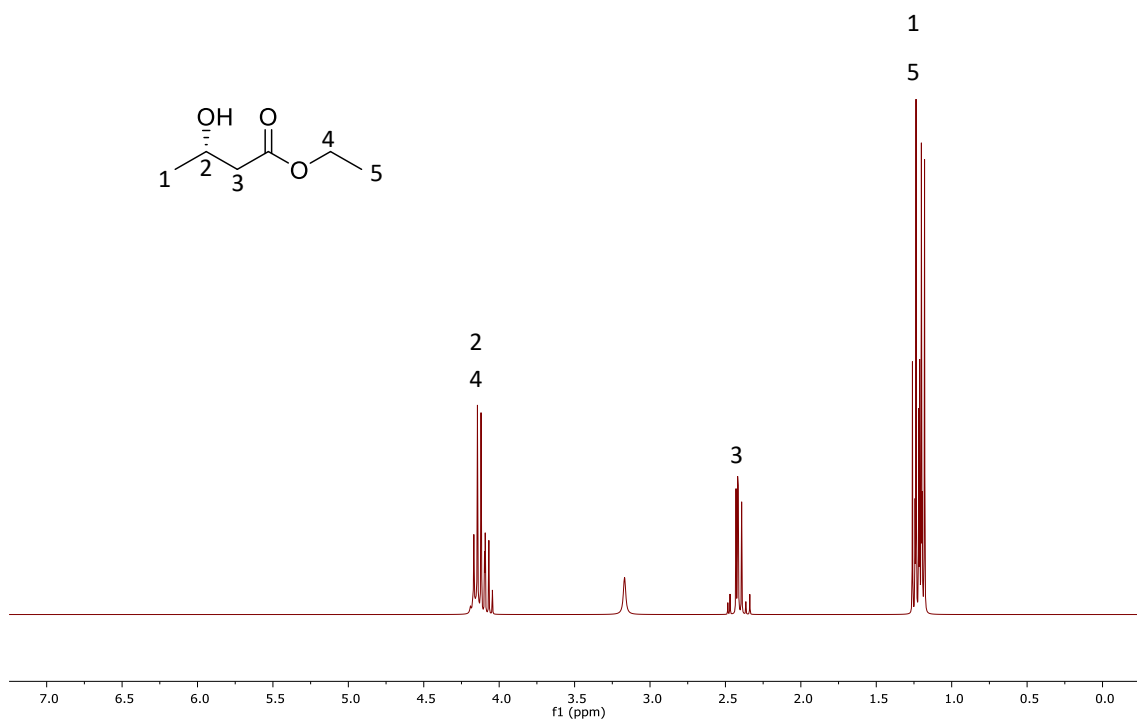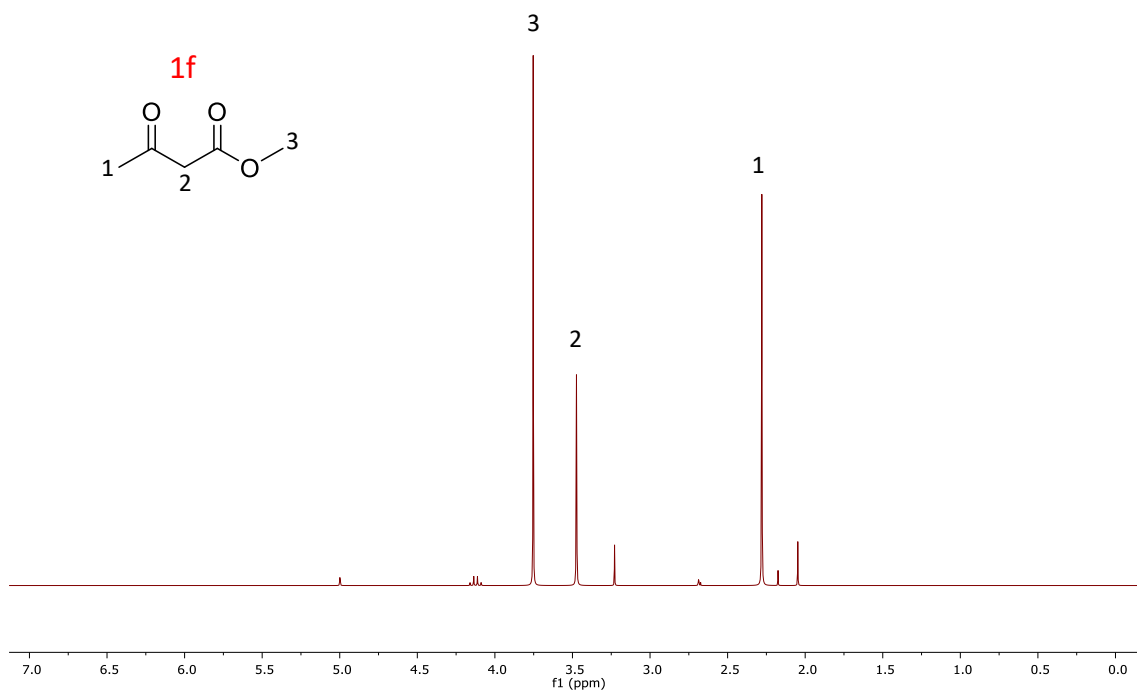
Figure S13. ¹H NMR of purified ethyl (*S*)-3-hydroxybutyrate (2a) (300 MHz, Chloroform, 298 K)

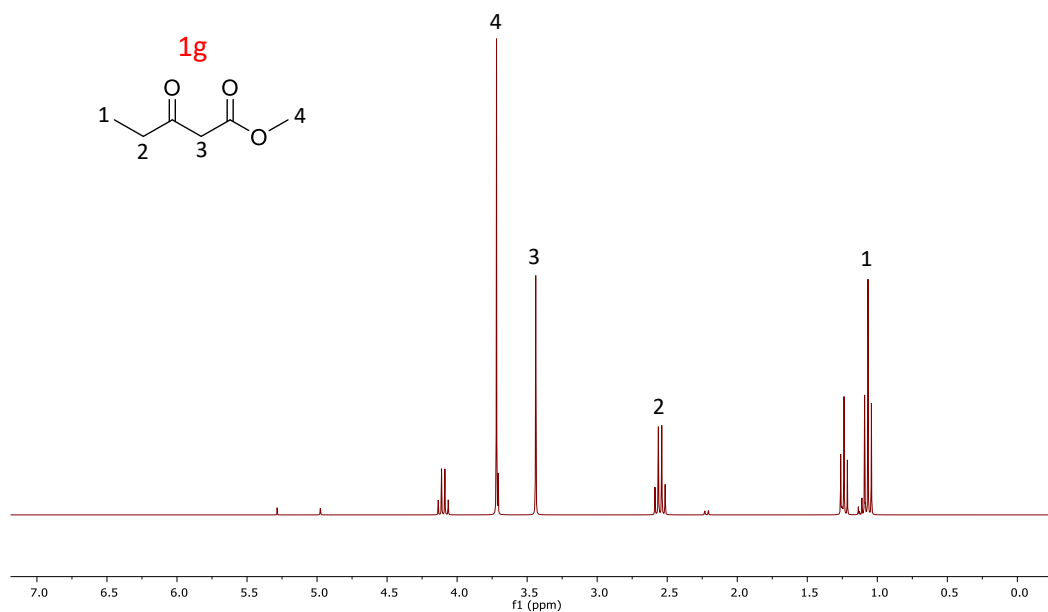¹H NMR (300 MHz, Chloroform, 298 K) δ 4.22 – 4.03 (m, 3H), 2.49 – 2.32 (m, 2H), 1.28 – 1.14 (m, 6H).
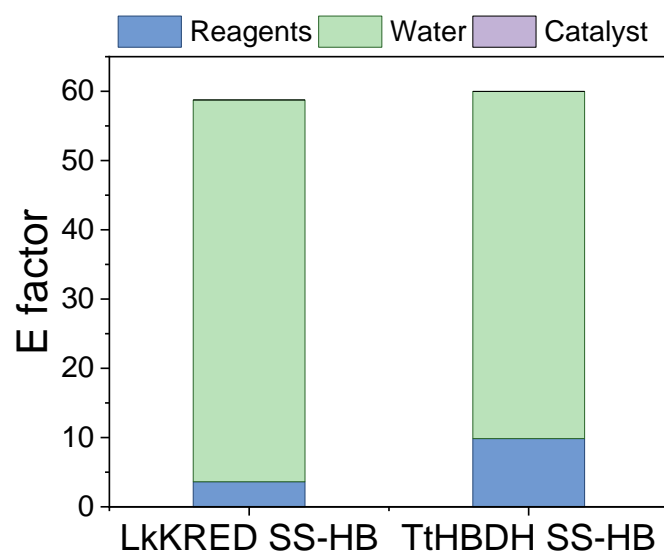
Figure S14. Dissected E factor

Dissected E factor of the continuous synthesis of *R*- and *S*- enantiomers of ethyl 3-hydroxybutyrate (2a) by TtHBDH and LkKRED ssHBs in continuous flow operation.
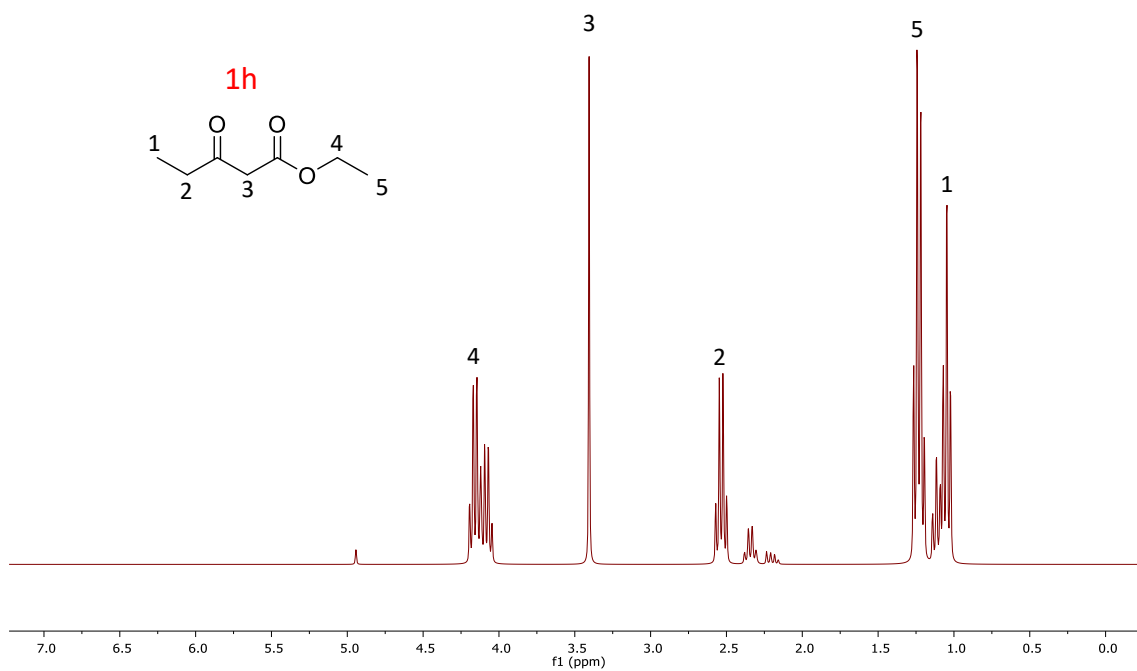
Figure S15. ¹H NMR of 1f (300 MHz, Chloroform, 298 K)

¹H NMR (300 MHz, Chloroform, 298 K) δ 3.75 (s, 3H), 3.47 (s, 3H), 2.28 (s, 3H).

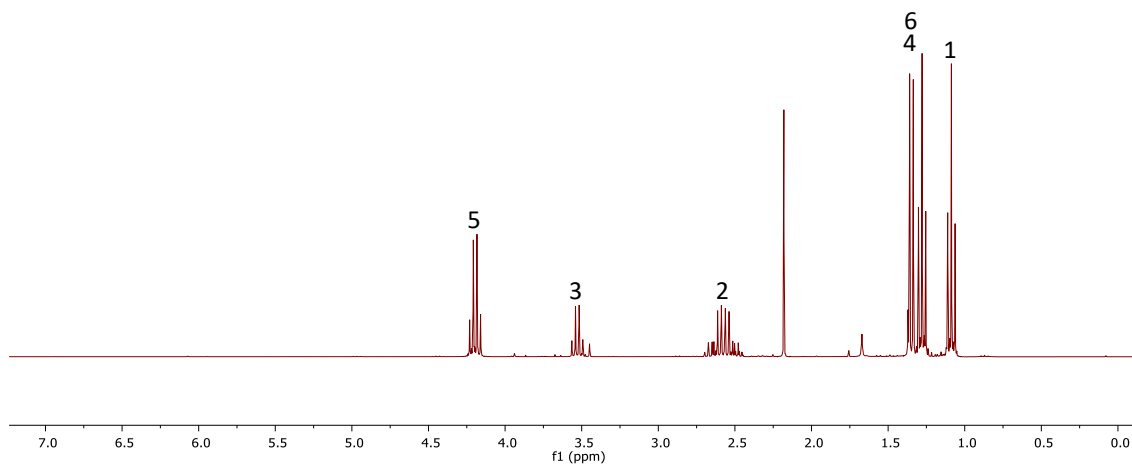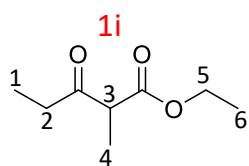**Figure S16. ^{1}H NMR of 1g (300 MHz, Chloroform, 298 K)**

^{1}H NMR (300 MHz, Chloroform, 298 K) δ 3.72 (s, 3H), 3.44 (s, 2H), 2.55 (q, *J* = 7.3 Hz, 3H), 1.07 (t, *J* = 7.3 Hz, 3H).

64

Figure S17. ^{1}H NMR of 1h (300 MHz, Chloroform, 298 K)

δ 4.16 (q, *J* = 7.2 Hz, 2H), 3.41 (s, 2H), 2.54 (q, *J* = 7.1 Hz, 2H), 1.24 (t, *J* = 7.1 Hz, 3H), 1.05 (t, *J* = 7.7 Hz, 3H).

Figure S18. ^{1}H NMR of 1i (300 MHz, Chloroform, 298 K)

δ 4.20 (q, J = 7.1 Hz, 2H), 3.59 – 3.42 (m, 1H), 2.71 – 2.43 (m, 2H), 1.38 – 1.20 (m, 6H), 1.07 (d, J = 7.2 Hz, 3H).

REFERENCES

1. A. H. Orrego, D. Andrés-Sanz, S. Velasco-Lozano, M. Sanchez-Costa, J. Berenguer, J. M. Guisan, J. Rocha-Martin and F. López-Gallego, *Catalysis Science & Technology*, 2021, **11**, 3217-3230.
2. A. Weckbecker and W. Hummel, *Biocatalysis and Biotransformation*, 2006, **24**, 380-389.
3. R. A. Cacho, J. Thuss, W. Xu, R. Sanichar, Z. Gao, A. Nguyen, J. C. Vederas and Y. Tang, *Journal of the American Chemical Society*, 2015, **137**, 15688-15691.
4. M. Lee, H. Jung, D. Kim, J.-W. Park and S. Chang, *Journal of the American Chemical Society*, 2020, **142**, 11999-12004.
5. J. Guisán, *Enzyme and Microbial Technology*, 1988, **10**, 375-382.
6. E. Diamanti, J. Santiago-Arcos, D. Grajales-Hernández, N. Czarnievicz, N. Comino, I. Llarena, D. Di Silvio, A. L. Cortajarena and F. López-Gallego, *ACS Catalysis*, 2021, **11**, 15051-15067.
7. G. García-Marquina, J. Langer, M. Sánchez-Costa, G. Jiménez-Osés and F. López-Gallego, *ACS Sustainable Chemistry & Engineering*, 2022, **10**, 9899-9910.